2008

Variational Study of the Nematic State of the Two Dimensional Electron Gas in a Magnetic Field

Quoc M. Doan

FLORIDA STATE UNIVERSITY

COLLEGE OF ARTS AND SCIENCES

VARIATIONAL STUDY OF THE NEMATIC STATE OF THE TWO DIMENSIONAL ELECTRON GAS IN A MAGNETIC FIELD

By

QUOC M. DOAN

A Dissertation submitted to the
Department of Physics
in partial fulfillment of the
requirements for the degree of
Doctor of Philosophy

Degree Awarded:
Spring Semester, 2008

The members of the Committee approve the dissertation of Quoc M. Doan defended on February 19, 2008.

Efstratios Manousakis
Professor Directing dissertation

Michael Mascagni
Outside Committee Member

Kun Yang
Committee Member

Jorge Piekerawicz
Committee Member

Peng Xiong
Committee Member

Approved:

Mark Riley, Chair
Department of Physics

Joseph Travis, Dean, College of Arts and Sciences

The Office of Graduate Studies has verified and approved the above named committee members.

I wish to dedicate this thesis to my parents for their love, support and faith in me.

ACKNOWLEDGEMENTS

I would like to thank my supervisor and major professor, Dr. Efstratios Manousakis, for his supervising, endless patience, help and support. I am really indebted to him, without his help and patience, it would be impossible for me to finish this great project.

I wish also to thank Dr. Kun Yang, Dr. Jorge Piekarewicz for being wonderful teachers, for their inspiring lectures and for serving on my committee. I would like to acknowledge my gratitude to my committee members, Dr. Peng Xiong, Dr. Michael Mascagni.

I really enjoy the atmosphere at this great physics department. Thanks to Sherry Tointigh for her assistance during my graduate study. Thanks also the other staff members for their warm hospitality.

This research was supported in part by the Department of Physics, and the Center for Materials Research and Technology, Florida State University.

TABLE OF CONTENTS

LIST OF TABLES

LIST OF FIGURES

ABSTRACT

We have studied the nematic state of the two dimensional electron gas (2DEG) at half-filled Landau level (LL). Our motivation comes from experiments in which anisotropic transport in the 2DEG under high magnetic field and at low temperature was observed. Based on a model of the nematic state proposed by Oganesyan, Fradkin and Kivelson, we investigate this state and compare it with other competing states proposed by other groups. First, we investigate at what LL the nematic state becomes energetically favorable as compared to the isotropic state. Our studies indicate that this occurs at the second excited LL. Moreover, we compare the energy of the nematic state with that of the stripe state obtained within the Hartree-Fock approximation (HF) and we conclude that, for the samples studied experimentally, the nematic state might be more stable. In our study we have used two different methods which both have advantages and disadvantages. The first method used is the Fermi-hyper-netted chain (FHNC) which provides results valid in the thermodynamic limit (infinite size system), however, it is accurate only for a low density system. The second method used is the Monte Carlo method (MC) which can be used on a finite-size system and, thus, the issue arises of how to extrapolate in the thermodynamic limit (finite-size effect). The results obtained from both methods are in good agreement and indicate that the nematic state might be a viable candidate to explain the experimental findings. In order to compare our results for the nematic state to those obtained for the stripe state, we needed to include the kinetic energy contribution beyond the familiar $\hbar\omega_c/2$ term in the case of the nematic state which comes from the deformed geometry of the Fermi sea. For the stripe state we have carried out a HF calculation for a more realistic potential for a 2DEG which includes the effects of the finite confinement of the electron wave function along the z-direction.

CHAPTER 1

INTRODUCTION

During the past two decades, the fractional quantum Hall effect (FQHE) has been one of the most intriguing research topics in condensed matter. The effect was observed at a certain filling factor of $1/m$ where m is odd. More recently, the measurements of Lilly et al. [2] and Du et al. [3] reveal a strong anisotropic behavior of transport properties of electrons for the half-filled Landau-level system under strong magnetic field and at very low temperature. The anisotropy commences at the second excited LL and persists up to the sixth excited LL. The sudden exhibition of large anisotropies of resistivities in clean 2DEG suggests that there is an unknown underlying microscopic origin for this kind of spontaneous symmetry breaking.

These experimental findings prompted several interesting theoretical proposals which attempt to explain the observed anisotropic behavior of the half-filled LL system. First of all, these anisotropic transport properties are consistent with already predicted stripe and bubble charge-density-wave phases found [4] [5] by means of Hartree-Fock calculations of the 2DEG. However, Fradkin and Kivelson [6] suggested that the anisotropic transport might be due to a stripe nematic phase of the 2DEG in a high magnetic field. This point of view was investigated further by Fradkin et al. [7] where a model for the nematic phase in a symmetry-breaking field was studied using Monte Carlo simulation. The results of the Monte Carlo simulation provide a good fit of the experimental data of Lilly et al. [2]. This simulation suggests that the nematic phase might be a good candidate to explain the anisotropic behavior observed in Refs. [2] and [3]. Furthermore, by deriving a long-wavelength elastic theory of the quantum Hall smectic state, Wexler and Dorsey [8] have estimated the transition temperature from an isotropic to nematic phase to be of the order of 200 mK. Later, Cooper et al. [9] by applying an in-plane magnetic field in 2DEG samples

which show the above anisotropy in transport, give further support for the possible presence of such a quantum nematic phase. In the composite fermion theory given by Jain [10] the fractional quantum Hall effect is interpreted as the integer quantum Hall effect of composite fermions. Furthermore, Halperin et al. [11] developed a theory of half-filled LL system, which is the case of our interest, as a compressible Fermi liquid. Rezayi and Read [12] proposed a ground-state wavefunction for the half-filled LL system having the Jastrow-Slater form as follows:

$$\Psi\left(\vec{r}_1,\vec{r}_2,...,\vec{r}_N\right)=\hat{P}_0\prod_{j<k}^{N}(z_j-z_k)^2 e^{-\sum_{k=1}^{N}|z_k|^2\Big/4}\det\left|\varphi_{\vec{k}}(\vec{r}_i)\right| \tag{1.1}$$

In equation (1.1), $\hat{P}_0$ is the projection operator onto the lowest LL, $\phi_{\vec{k}}(\vec{r}_i)$ are two-dimensional (2D) plane-wave states. Here, $z_j = x_j + iy_j$ is the complex 2D coordinate of the j electron. This wavefunction is a Jastrow correlated Slater determinant with Jastrow part similar to the Laughlin state [13].

Ciftja and Wexler [14] used the Fermi-hypernetted-chain (FHNC) approximation to study a broken rotational state of the half-filled LL where the symmetry-breaking parameter was introduced in the correlation part of the wavefunction; namely, the Jastrow factor was modified as$(z_i - z_j)^2 \rightarrow (z_i - z_j - \alpha)(z_i - z_j + \alpha)$, and the single-particle determinant was the standard circular Fermi sea. The anisotropy symmetry-breaking parameter α is determined by minimizing the ground-state energy.

In this thesis, we adopt the ansatz for the ground state of the nematic state proposed by Oganesyan et al. [15] as a trial wavefunction in our variational calculations. The ground-state wavefunction proposed in Ref. [15] has the same form as the wavefunction given by Eq. (1.1); however, the single-particle momenta form an elliptical Fermi sea as opposed to the circular Fermi sea. The broken-symmetry parameter in our problem is the ratio $\alpha = k_1/k_2$ of the semimajor k_1 and semiminor k_2 axes of the elliptic Fermi sea. We will study the nematic state of the half-filled LL system using the variational approach and we will employ the Fermi-hypernetted-chain approximation and Monte Carlo approximation. Namely, we investigate whether or not this state, in which the anisotropy is due to an elliptical Fermi sea, can be energetically favorable relative to the isotropic state and the stripe ordered Wigner crystal at high LL. We find that the nematic phase can be stabilized against the isotropic case beyond the second excited LL. In addition, we have compared the energy of the nematic state

to that obtained by a self-consistent Hartree-Fock calculation [5] of the stripe and bubble states of the 2DEG. We find that there is a transition between the stripe ordered ground state and the nematic phase as a function of the parameter λ of the interaction used by Zhang and Das Sarma [16] to take into account the finite layer thickness. In particular, for the case of the materials [2], [3] in question, we find that the ground state corresponds to the nematic state.

In this work, we only consider the unprojected wavefunction of the nematic state. We assume that the unprojected wave function is a good approximation to the real wavefunction for the lowest Landau level. Moreover, it is known that the projection operator almost eliminates the high LL components of the wavefunction [17]. The advantage of this unprojected version is that it has a Jastrow form with a Slater determinant so it can be applied directly with FHNC. In addition, the use of this simplified wavefunction allows us to study large-size systems using the variational Monte Carlo method.

This thesis is organized as follows. In chapter 2, we introduce the FQHE and salient points of the picture of the FQHE ground state developed by Laughlin; the results of the study of the Laughlin state using the hypernetted chain (HNC) and MC for a system with toroidal boundary conditions are also reported. In chapter 3, the experimental results of Lilly et al. [2], in which the anisotropic behavior of the half-filled LL system was observed, will be briefly presented. Chapter 4 is a brief review of the composite fermion picture of Jain, and the mean field approximation carried out by Halperin et al. [11] which showed that at half-filling factor the 2DEG can have a Fermi sea. In addition, the ground state wavefunction proposed by Rezayi and Read [12] for the isotropic half-filled case is discussed. A model of nematic state by Fradkin and Kivelson will also be discussed. In chapter 5, we will describe how we study the nematic state using FHNC. The ansatz ground state wavefunction we use is the one suggested by Oganesyan et al. [15]. We present our results and we compare them with those of the stripe state obtained by using HF. In chapter 6 we will describe our MC simulation method implemented for the toroidal geometry. The results we obtain using MC are in general agreement to those obtained from FHNC. In chapter 7 we will briefly discuss our implementation of the HF approximation [4], [5] for the stripe state in the case where we use a more general interaction potential which incorporates the effect of the finite confinement of the wavefunction along the z-direction [16]. In this thesis for easy reference, we will refer to this potential as the Zhang-Das Sarma (ZDS) interaction.

The results obtained in chapter 7 for the stripe state are compared with the results obtained for the nematic states by MC and FHNC. In chapter 8 we present a summary of our results and conclusions.

CHAPTER 2

Fractional Quantum Hall Effect

In this section we will briefly review the FQHE and discuss the ground state wavefunction of a FQHE system proposed by Laughlin. The Laughlin's picture provides us many insights about the behavior of a 2DEG under a strong perpendicular magnetic field. His original theory serves as a major source of intuition for many following theoretical works about FQHE-related systems. That is why it is worthwhile to review some salient points of his description of the ground state of FQHE.

The two most common computational methods used to study FQHE are the hyper-netted chain (HNC) and MC. Laughlin in his original works of FQHE in Ref. [13] used the HNC to obtain the pair distribution function and the interaction energy. Morf and Halperin in Ref. [1] used the MC with the disk geometry and free boundary conditions, and obtained similar results. In our work we also use these two methods to study the nematic state of a 2DEG, so it is necessary to discuss how to implement them for the FQHE and verify the results with the ones obtained by other groups.

In section 2.1 we will briefly describe the FQHE and the ground state wavefunction proposed by Laughlin. In section 2.2 we will discuss how to implement the HNC to study FQHE state and compare the results with other groups. In section 2.3, we will show that with an alternative MC using the square geometry with periodic boundary conditions, one can obtain results which are almost the same as those obtained by Morf and Halperin.

2.1 FQHE and the Laughlin theory of the ground state of FQHE

The fractional quantum Hall effect (FQHE) occurs in a high-mobility AlGaAs/GaAs heterojunction (e.g Refs. [18], [19], [20] and [21]) and in high-mobility Si-MOSFETs (e.g

Refs. [22] and [23]) under a high magnetic field (about 2 T) and at a very low temperature (about 250 mK). Under these conditions, the diagonal resistivity ρ_{xy} presents some plateaus quantized to a certain simple fraction ν of the unit e^2/h and at the same places the transversal component of resistivity ρ_{xx} is almost zero. Fig. 2.1 originally obtained by Tsui et al. in [24] illustrates the effect:

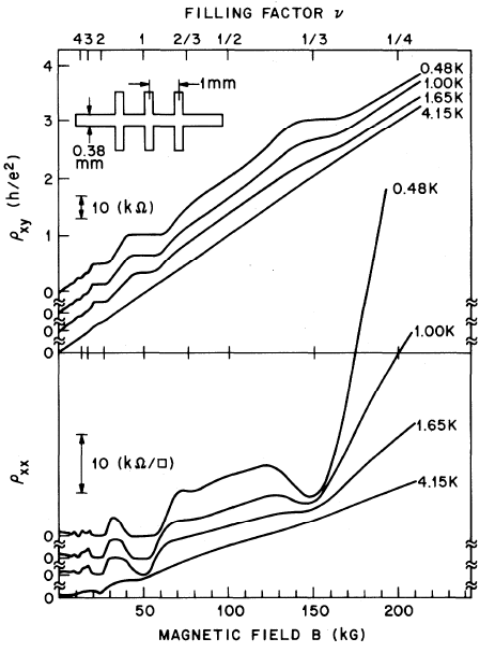

Figure 2.1: The Hall resistivity ρ_{xy} and the diagonal resistivity ρ_{xx} as a function of a magnetic field in as GaAs-heterojunction with electron density $n_o = 1.23 \times 10^{11}/cm^2$.

In later experiments, the quantization of the plateau was found to be better than 3 parts in 10^5 with ρ_{xx} lower than 0.1Ω in much higher-mobility samples. Most surprisingly, the effect occurs only at particular values of filling factor of Landau level $\nu = 1/m$ where m is an odd number. So far, the value of filling factor ν observed in FQHE includes (Refs. [25] and [26]):

$$\nu = \frac{1}{3}, \frac{2}{3}, \frac{4}{3}, \frac{5}{3}$$
$$\nu = \frac{1}{5}, \frac{2}{5}, \frac{3}{5}, \frac{4}{5}, \frac{7}{5}, \frac{8}{5}$$
$$\nu = \frac{2}{7}, \frac{3}{7}, \frac{4}{7}, \frac{5}{7}, \frac{10}{7}, \frac{11}{7}$$

and several filling factors with values of denominator are $9, 11, 13, 15$.

The development of these characteristics in FQHE is very similar to the one in which the quantized Hall resistance ρ_{xy} and vanishing ρ_{xx} observed at integral values of filling factor ν (Integral Quantum Hall Effect IQHE). The IQHE can be explained by Laughlin [27] using the gauge invariance given the complete occupation of the Landau levels. In the case of FQHE, the Landau level is only partially occupied so the above arguments cannot be applied. In contrast, the correlation between the electrons plays an essential role for the FQHE. Laughlin in [13] proposed a very fundamental ground state picture of FQHE. This picture was later elaborated by himself in [28] and other authors in [29] and [1]. For a 2DEG with filling factor $\nu = 1/m$, the ground state wavefunction proposed by him in [13] has the following form:

$$\psi_m = \prod_{j,k=1\, j<k}^{N_e} (z_j - z_k)^m \prod_{j=1}^{N_e} e^{-|z_j|^2/4l_0^2} \tag{2.1}$$

where N_e is the number of particles, $z = x - iy$ is the complex coordinate of the particle, l_0 is the magnetic length, and given by $\sqrt{\frac{\hbar c}{eB}}$.

This wavefunction has very important following properties:

1. The particles tend to keep a certain distance from each other. When two particles approach each other, the wavefunction goes to zero as power of m. Thus, the wavefunction tends to minimize the interaction energy.

2. This wavefunction consists of only single-particle wavefunctions at the lowest LL.

3. Comparison of these wavefunctions with the exact wavefunctions obtained for the cases of small numbers of particles shows that they almost overlap (see Ref. [30]).

4. For m being an odd integer, this wavefunction obeys Fermi statistics.

5. This wavefunction is an eigenstate of the total angular momentum with eigen value of $M = \frac{N_e}{2}(N_e - 1)m$.

To have a better of understanding of this wavefunction, one can map it into the problem of a 2D one-component plasma. Specifically, the square of the wavefunction can be interpreted classically as a probability distribution function as follows:

$$|\psi_m|^2 = e^{-H_m}, \tag{2.2}$$

where, obviously:

$$H_m = -2m \sum_{j<k} ln|z_k - z_k| + \sum_{j=1}^{N_e} |z_j|^2/2{l_0}^2. \tag{2.3}$$

This has a form of the Hamiltonian of a neutral classical 2-dimensional plasma with particle charge e embeded in the uniform background charge of density ρ_m [31], where:

$$e^2 = 2m, \rho_m = \frac{1}{2\pi l_0^2 m} \tag{2.4}$$

In the Hamiltonian in equation (2.3), the first term is the Coulomb interaction between particles in 2D, and the second term is the interaction between particles and the uniform background charge. The interaction energy per particle can be calculated via the pair distribution function as follows:

$$E = \frac{\rho}{2} \int [v(\vec{r}) - 1] g(\vec{r}) d^2 r \tag{2.5}$$

where $v(\vec{r})$ is the 2-body interaction potential and $g(\vec{r})$ is the pair distribution function. The above interaction energy includes both the particle-particle and the particle-background charge interaction. One of the most important behaviors of 2D one component plasma is that, the particles tend to uniformly spread out. Remember that in the Laughlin description of FQHE, we assume that the Coulomb interaction is small compared to the cyclotron kinetic energy so that the LLs do not mix when we include the Coulomb interaction, or in other words, the band structure of LL is still intact when we turn on the Coulomb interaction between particles. As a consequence, the kinetic energy is totally quenched so the physics is totally determined by the Coulomb potential interaction. Having equated the problem of FQHE with the problem of 2D one-component plasma (2D OCP) one can study it using computational methods applied for 2D OCP. In his paper, Laughlin used the Hypernetted chain (HNC) to obtained the pair distribution functions. Morf and Halperin [1] also used the Monte Carlo (MC) method with disk-geometry to study it. In the next two sections, we will discuss the implementations of HNC and MC to study the FQHE state.

2.2 HNC study of the FQHE state

The HNC method was applied successfully to study classical plasma [32] and quantum fluid [33]. To study the FQHE, we follow the HNC recipe which outlined in detail in [30]

and [34]. In HNC, one solves the following set of equations to obtain the pair distribution function $g(\vec{r})$:

$$g(\vec{r}) = exp(N(\vec{r}) - u(\vec{r})), \tag{2.6}$$

$$\tilde{N}(\vec{q}) = \frac{\tilde{X}(\vec{q})^2}{1 - \tilde{X}(\vec{q})}, \tag{2.7}$$

$$X(\vec{r}) = g(\vec{r}) - 1 - N(\vec{r}). \tag{2.8}$$

In the above equations, $\tilde{X}(\vec{q})$ is the Fourier transform of $X(\vec{r})$. In 2D, the Fourier transform of a given function $f(r)$ is given by:

$$\tilde{f}(q) = 2\int_0^\infty f(r)J_0(qr)rdr, \tag{2.9}$$

where $J_0(x)$ is the first-kind Bessel function of zero order. $u(r)$ is the pseudo-potential and given by:

$$u(r) = -2mln(r). \tag{2.10}$$

Remember that our FQHE state under consideration has the spherical symmetry so we can drop the vector sign in the HNC equations. Since the pseudo-potential is a logarithmic interaction, one can split it into short-range and long-range part as follows:

$$u^s(r) = 2mK_0(Qr), \tag{2.11}$$

$$u^l(r) = -2m[ln(r) + K_0(Qr)], \tag{2.12}$$

where $K_0(x)$ is the modified second-kind Bessel function of zero-order and Q is a cut-off parameter of order unity (of course, the final results do not depend on Q). Then, we can define new set of short-range functions:

$$N^s(r) = N(r) - u^l(r), \tag{2.13}$$

$$X^s(r) = X(r) + u^l(r). \tag{2.14}$$

And, the final set of equations can be expressed via these new short-range functions as follows:

$$\tilde{N}(q) = \frac{\tilde{X}^s(q)[\tilde{X}^s(q) - \tilde{u}^l(q)] - \tilde{u}^l(q)}{1 - \tilde{X}^s(q) + \tilde{u}^l(q)}, \tag{2.15}$$

$$\tilde{u}^l(q) = \frac{4mQ^2}{q^2(q^2 + Q^2)}, \tag{2.16}$$

$$g(r) = exp[N^s(r) - u^s(r)], \tag{2.17}$$

$$X^s(r) = g(r) - 1 - N^s(r). \tag{2.18}$$

Table 2.1: Interaction energies of the FQHE system with several different filling factor $1/m$.

Filling factor $\nu = 1/m$	Energy (in units of e^2/l_0)
$m = 1$	-0.622251
$m = 3$	-0.40541
$m = 5$	-0.323969

Solving these equations iteratively, we obtain the pair distribution function. The self-consistence is usually achieved after 100 iterations. The initial value of $N^s(r)$ is set to 0. In Fig. 2.2, we display the pair distribution function obtained for several filling factors $1, 1/3, 1/5$. One can see from this figure that the FQHE system has a liquid-like pair distribution function. The corresponding interaction energies are given in table 2.1. These values agree very well with the results in Ref. [34].

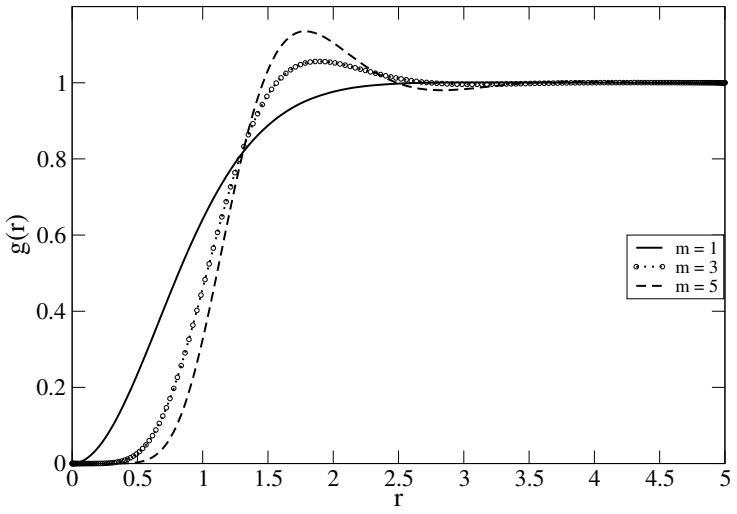

Figure 2.2: Pair distribution function $g(r)$ for the FQHE system with several filling factor of $\nu = 1/m$.

2.3 MC study of FQHE

In [1] Morf et. al. studied a FQHE state with filling factor 1/3 using a Monte Carlo method with the disk-geometry. As a preliminary test, we also use MC to study it, but our geometry is a square with periodic boundary conditions. The reason we want to use this geometry is because it is more natural to adapt to the case of the nematic state as discussed in chapter 6. First, we map the FQHE problem into the problem of a 2-D one component plasma as discussed in section 2.1. In addition, due to the long range 2-body potential interaction $u(r) = -lnr$, one needs to take into account all the interactions of particles in the basic cell with all other cells to obtain a realistic model for the physical system. But such a procedure will waste computing time. One conventional treatment for this difficulty comes from the solution to compute lattice sums introduced by Ewald. The main idea is, instead of calculating the all image charge interactions from other cells, we calculate the charge interaction only in the basic cell by solving the Poisson equation with periodic boundary conditions.

The general Poisson equation in 2D is given by:

$$\nabla^2\phi(\vec{r}) = -2\pi\rho(\vec{r}) \tag{2.19}$$

where $\phi(\vec{r})$ is the electric potential at $\vec{r}$ due to a particle at the origin, and $\rho(\vec{r})$ is the charge density. The boundary conditions imposed on $\phi(\vec{r})$ and $\rho(\vec{r})$ are the periodic boundary conditions, namely:

$$\phi(\vec{r}) = \phi(\vec{r} + \vec{L}), \tag{2.20}$$

$$\rho(\vec{r}) = \rho(\vec{r} + \vec{L}), \tag{2.21}$$

where $\vec{L}$ is the size of the basic cell.
The charge density in the basic cell of area A is given by:

$$\rho(\vec{r}) = e\delta(\vec{r}) \tag{2.22}$$

First, we expand $\phi(\vec{r})$ and $\rho(\vec{r})$ in Fourier series as follows:

$$\phi(\vec{r}) = (1/A)\sum_{\vec{k}} \phi_{\vec{k}} e^{i\vec{k}\cdot\vec{r}}, \tag{2.23}$$

$$\rho(\vec{r}) = (1/A)\sum_{\vec{k}} \rho_{\vec{k}} e^{i\vec{k}\cdot\vec{r}}, \tag{2.24}$$

and $\rho_{\vec{k}}$ is given by:

$$\rho_{\vec{k}} = \int_A \rho(\vec{r}) e^{-i\vec{k}\cdot\vec{r}} d^2r. \tag{2.25}$$

In the above equations, wave vectors $\vec{k}$ are defined for a finite box with length of L by:

$$\vec{k} = 2\pi\vec{n}/L, \tag{2.26}$$

$$\vec{n} = (n_x, n_y), \tag{2.27}$$

where n_x and n_y are integer numbers. Then one can derive that:

$$\rho(\vec{r}) = \frac{e}{A} \sum_{\vec{k}\neq 0} e^{i\vec{k}\cdot\vec{r}} \tag{2.28}$$

In the sum above, we omit the component corresponding to $\vec{k} = 0$ since it corresponds to the uniform background charge. Plugging equation (2.23) and (2.28) into the Poisson equation (2.19), and equating coefficients containing the same values of $\vec{k}$, one can easily obtain:

$$\phi_{\vec{k}\neq 0} = \frac{2\pi e}{k^2}. \tag{2.29}$$

Thus:

$$\phi(r) = \frac{2\pi e}{A} \sum_{\vec{k}\neq 0} \frac{e^{i\vec{k}\cdot\vec{r}}}{k^2} \tag{2.30}$$

In the case of FQHE, the particle charge e is defined by $e^2 = 2m$ then the potential interaction is:

$$u(r) = \frac{4m\pi}{A} \sum_{\vec{k}\neq 0} \frac{e^{i\vec{k}\cdot\vec{r}}}{k^2} \tag{2.31}$$

Expression (2.31) will be used as the pseudo-potential in our MC calculation.

We run the MC simulation for systems of 55 and 89 particles. We found that there is no noticeable difference in results for 55 and 89 particles. The sum over $\vec{k}$ in equation 2.31 is carried out for 200 k-states. The number of MC steps for "thermalization" is $100,000$ and for averaging the pair distribution function is $2,000,000$. This guarantees that averaging of the pair distribution function converges.

In Fig. 2.3 we compare our pair distribution function with the one obtained by Morf and Halperin in [1]. It shows that they are almost the same. Next, we calculate the interaction energy. Our result for the interaction energy, -0.410605 ($e^2/\epsilon l_0$), is also in very good agreement with [1], -0.410 $\pm$0.001 ($e^2/\epsilon l_0$). This result convinces us to use the same MC

approach to study the nematic state. In the next chapter, we will describe the experiment in which the anisotropy of transport properties of a 2DEG was observed. The results of this experiment are our main motivation.

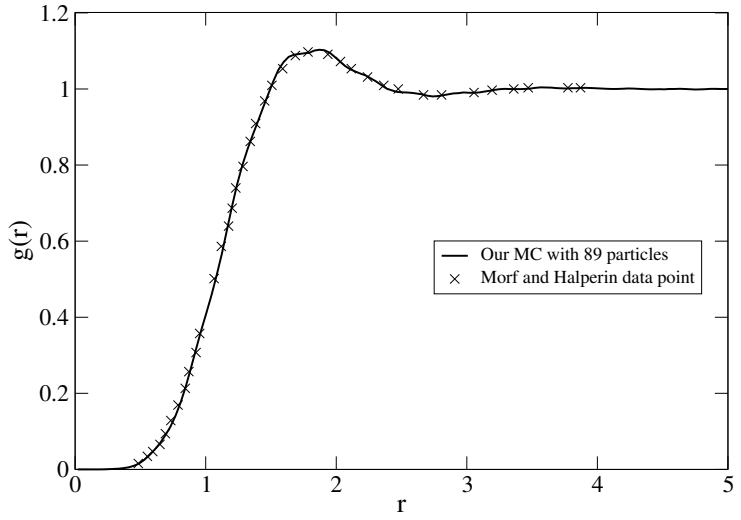

Figure 2.3: Comparison of the pair distribution functions done for 1/3 system by our MC and [1]

CHAPTER 3

Evidence for an Anisotropic State of Two-Dimensional Electrons in High Landau Levels

In this chapter, we will describe the experiments done by Lilly et al. [2] in which they observed a anisotropy of the transport properties of 2DEG at high LL level at low temperature. The samples used in this experiment are GaAs/AlGaAs heterojunction wafers. There are six samples: A,B,C,D,E and F with different electron density. They were rotated to ensure a high homogeneity of the density. These densities for samples A, B, and C (in units of $10^{11}cm^{-2}$) are close to $n_s = 2.67$; $n_s = 2.27$ for samples D and E; and $n_s = 1.52$ for sample F. The low temperature mobility of each sample is $\mu \geq 9 \times 10^6 cm^2/Vs$. Under a high magnetic field and at low temperature, measurements of resistivities ρ_{xx} for these samples were conducted. Fig. 3.1 taken from [2] illustrates the finding of anisotropy of ρ_{xx}.

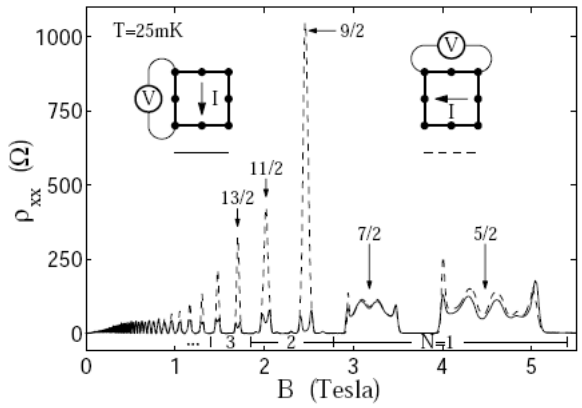

Figure 3.1: Anisotropy of ρ_{xx} in sample A at $T = 25mK$. The two traces (dash and solid trace) result from simply changing the direction of current through the sample; the sample itself is not rotated.

The two traces are the resistance of sample A measured at $T = 25mK$ along two perpendicular directions of the current going through the sample while the sample itself is not rotated. At $\nu = 9/2$ the ratio between two resistances is close to 100. This anisotropy persists from $N = 2$ LL to $N = 6$ LL. However, at $N = 1$ and $N = 0$ there is no such effect. The anisotropy is confined to the centers of LLs which correspond to the half-filled LL system. Away from that, the two traces basically match. When the temperature is increased, the effect becomes less pronounced, and at $T = 150mK$ it is no longer noticeable. The principle axes of the anisotropy are found to be roughly parallel to the sides of the chip for sample A. When same measurements are done on other samples with different densities and configurations, similar results were also observed.

This sudden development of the anisotropy at the 2^{nd} excited LL and higher LL suggests that there is some underlying origin that has not been accounted for. The results of this discovery are the motivation for a several theoretical works that investigate what state is accounting for this anisotropic behavior. In the following chapter, we will first describe the ground state of 1/2-filled system, followed by some salient points of the nematic state of 2DEG which is a candidate for the observed anisotropic state.

CHAPTER 4

Nematic state as ground state of half-filled LL system

A theoretical study of the half-filled LL system was carried out by Halperin, Lee and Read [11] in which each electron can carry two flux quanta. The idea of transforming each electron into a new particle carrying flux quanta was developed by Jain [10]. This new particle is called composite fermion. According to Jain's picture, a FQHE system of electrons is described equivalently as of a IQHE system of composite fermions. In [12] Rezayi and Read proposed the ground state wavefunction for a 2DEG with filling factor of 1/2 based on this picture.

In [6] Fradkin and Kivelson introduced various electron liquid crystalline phases: quantum smectic, quantum nematic, quantum isotropic fluid, insulating stripe-crystal, and Wigner crystal. Oganesyan et. al. in [15] proposed that the transition from the isotropic to the nematic state is a Fermi-surface instability. They proposed a ground state wavefunction for the nematic state of 2DEG at half-filled LL based on the ground state wavefunction proposed by Rezayi and Read [12]. Fradkin et al. in [7] study the nematic state at finite temperature in a symmetry-breaking field using a Monte Carlo simulation. Their results provided a good fit with the data compiled from experiment of Lilly et al. [2].

In the next section we will briefly present the salient points of composite fermion picture proposed by Jain. Then in section 4.2, we will discuss about the study of half-filled LL system developed by Halperin et al. [11]. The ground state wavefunction for half-filled LL system proposed by Rezayi and Read [12] is also discussed. In section 4.3, we will introduce the electronic liquid-crystalline phases [6]. The results obtained by Fradkin et al. in Ref. [7] and the proposed ground state wavefunction of the nematic state in Ref. [15] will be briefly reviewed.

4.1 Theory of Composite Fermions

In an attempt to explain both IQHE and FQHE in an unified theoretical framework, Jain [10] developed a very simple picture of composite fermion (CF). Each electron carries an attached quantum magnetic flux and the number of flux quanta it carries is defined by the filling factor or electron density. In [35,36], it was shown that this can be done by using the Chern-Simon approach. In particular, one can introduce a Chern-Simons gauge field that interacts with the electrons or equivalently one can attach a "magnetic flux tube" to each electron (see [37]). In the following, we will present some important steps of this argument. For a detailed discussion of this approach, one can refer to Refs. [35,36].

First, consider the following vector potential for a single electron confined to the x-y plane:

$$\vec{\mathcal{A}} = \xi \frac{\hat{z} \times \vec{r}}{r^2} \tag{4.1}$$

The vector potential (4.1) is singular and clearly produces a magnetic field ($\vec{\bigtriangledown} \times \vec{A}$) which is zero every where except at the origin. The flux piercing through the origin can be obtained by:

$$\Phi = \oint \vec{\mathcal{A}} \cdot d\vec{l} = 2\pi\xi \tag{4.2}$$

This flux has a magnitude governed by ξ. For an integer number of flux quanta, ξ has to be $n\Phi_0/2\pi$, where n is integer, and $\Phi_0 = hc/e$ is the quantum of flux. With this gauge field, one can interpret that an electron moving in x-y plane can only experience the vector potential due to the flux piercing through the origin. For the case of N electrons, the vector potential (4.1) can be generalized as follows:

$$\vec{\mathcal{A}}_i = \xi \sum_{j \neq i}^{N} \frac{\hat{z} \times (\vec{r}_i - \vec{r}_j)}{(\vec{r}_i - \vec{r}_j)^2} \tag{4.3}$$

In this case, there is a flux tube of strength $2\pi\xi$ piercing at every position of electron j "seen" by electron i. Note that $\vec{\mathcal{A}}_i$ can be expressed as a gradient of a scalar $\vec{\mathcal{A}}_i = -\xi \bigtriangledown_i \theta_{ij}$ where the angle θ_{ij} is defined by $(z_i - z_j) = |z_i - z_j| e^{i\theta_{ij}}$. The Hamiltonian for the many-body system can be written as:

$$H = \frac{1}{2m} \sum_i (\vec{p}_i + e\vec{A}_i)^2 + \sum_{i<j} V(\vec{r}_i - \vec{r}_j) \tag{4.4}$$

where A_i is the vector potential at the position of electron i corresponding to a uniform external magnetic field pointing in the z-direction and $V(\vec{r}_i - \vec{r}_j)$ is the interaction energy between particle i and j. By a gauge transformation $\vec{A}'_i = \vec{\mathcal{A}}_i + \vec{A}_i$; one can find that the eigenstates of the Hamiltonian $H\prime$ (after the gauge transformation) can be written in terms of the eigenstates of the Hamiltonian H (before the gauge transformation) as follows:

$$\psi' = \prod_{i<j} \left(\frac{z_i - z_j}{|z_i - z_j|} \right)^{\eta} \psi \tag{4.5}$$

where ψ and ψ' are the eigen values for the case of the Hamiltonian before and after the Chern-Simon gauge transform correspondingly, and $\eta = e\xi/\hbar$ (for simplicity, we set $c = 1$). Although the Chern-Simon gauge field is singular, none of the physics has been altered, hence, all the measurable quantities remain unchanged. One can refer to [35] for more detailed discussions about the non-relativistic Chern-Simon gauge.

Using the model described above, Jain in [10, 38] constructed a trial wavefunction of the CF which is an electron with an even number of flux quanta attached to it. Since electrons are fermions then the wavefunction ψ is odd under exchange of 2 electrons, the statistical phase introduced by the flux must have even exchange symmetry. This can be done by setting $\xi = 2n\Phi_0/2\pi$ then $\eta = 2n$. Equivalently the wavefunction of CF is written as follows:

$$\psi_{2n} = \prod_{i<j} (z_i - z_j)^{2n} \psi \tag{4.6}$$

And as pointed out in [10, 38] this procedure allows us to produce all the essential physical features of the IQHE and FQHE within a unified framework.

First, one recalls the Laughlin wavefunction for $1/m$ filling FQHE system with m is odd:

$$\psi_{1/m}(\vec{r}) = \prod_{i<j}^{N_e} (z_i - z_j)^m e^{-|z_i|^2/4l_0^2} \tag{4.7}$$

This wavefunction can be rewritten as follows:

$$\psi_{1/m}(\vec{r}) = \prod_{i<j} (z_i - z_j)^{m-1} \psi_1(\vec{r}) \tag{4.8}$$

where $\psi_1(\vec{r})$ is the incompressible IQHE state at filling factor 1, and it has the following form:

$$\psi_1(\vec{r}) = \prod_{i<j} (z_i - z_j) e^{-|z_i|^2/4l_0^2} \tag{4.9}$$

One can interpret that the multiplying factor in (4.8) simply adds $m-1$ (even) flux quanta to each electron in the complete-filled LLL. The state ψ_1 is a state with one flux quanta per electron; the state $\psi_{1/m}$ is equivalent to a CF state with complete-filled LL in which each CF carries $m-1$ flux quanta. Thus, all the states of filling factor $1/m$ can be generated by building CF states of electrons in the lowest LL and adding an even number of flux quanta to each electron. It was also argued in [10] that this addition of flux quanta does not destroy the correlations in ψ_1 responsible for the incompressibility. Since Fermi statistics are responsible for the stability of ψ_1, and we do not change the exchange symmetries, the state $\psi_{1/m}$ is incompressible as well. As shown by Lopez et al. in Ref. [39], Jain's CF model describe a picture of the origin and properties of the Laughlin's wavefunction. It describes the FQHE as a manifestation of the IQHE for particles with an attached flux. For a detailed discussion of Jain's CF approach, one can refer to Ref. [36].

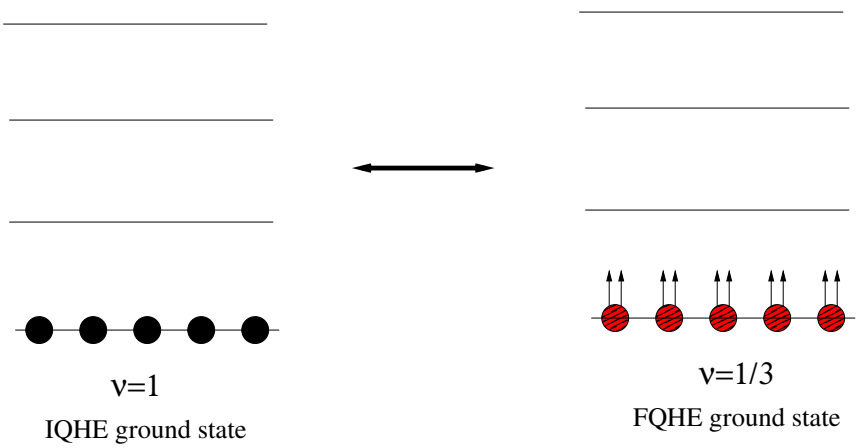

Figure 4.1: Schematic view of the ground state of electrons at $\nu = 1$ (on the left), and the ground state of CFs carrying two flux quanta (on the right) which corresponding to FQHE of electrons at filling factor $\nu = 1/3$.

4.2 CF picture for half-filled LL system

The CF picture for a 2DEG under a magnetic field provides us a simpler understanding of the wavefunctions associated with the incompressible states responsible for FQHE. However, when applied the idea of CF for the half-filled LL system, Halperin et al. [11] provide us a

very interesting picture about the CF's behavior. It was suggested in [10,13,40,41] that in a mean field approximation, each electron can "see" an average background flux due to other particles rather than individual flux tubes. This "mean" field is a fictitious field which is a result of the Chern-Simon gauge, and hence, it does not change the real field in the sample.

Consider the case corresponding to two flux quanta per electron. Then, the magnitude of corresponding "mean" field can be obtained by multiplying the electron density ρ_e (number of particle per unit area) with this number of flux quanta:

$$B_G = \rho_e \frac{2h}{e}. \tag{4.10}$$

On the other hand, from the definition of the filling factor:

$$\nu = \rho_e \phi_0 / B, \tag{4.11}$$

where B is the external magnetic field, one can derive the external magnetic field for a system of half-filling as:

$$B_{1/2} = \rho_e \frac{2h}{e}. \tag{4.12}$$

Thus, remarkably at half-field LL, if the effective field and the applied field are oppositely directed then we get a cancellation of the real and gauge field. In other words, CF particles are moving in zero average effective magnetic field. Therefore, this model predicts the existence of a Fermi surface of CF for a 2DEG at half-filled LL. In addition, CF particles at filling factor close to 1/2 undergo very large cyclotron orbits compared to those of electrons since the effective field $B_{eff} = B - B_{1/2}$ is much smaller than the real field B. These predictions are supported by many experiments [42,43].

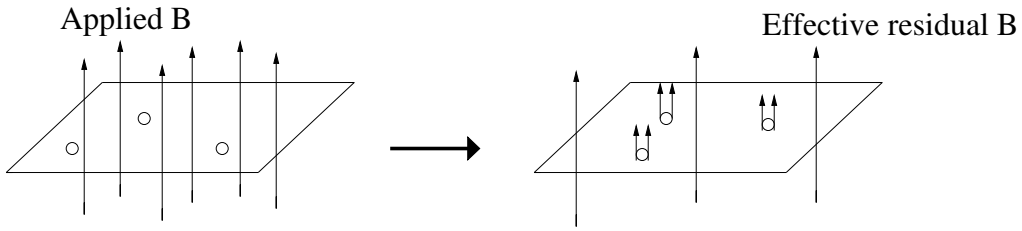

Figure 4.2: Each electron captures two flux quanta and becomes a CF. CFs experience an average residual magnetic field which is much smaller than the applied magnetic field.

Based on the CF picture of Jain and motivated by the Halperin et al. [11], Rezayi and Read in [12] proposed a trial ground state wavefunction for the 2DEG at half-filling as follows:

$$\psi_{1/2} = \hat{\mathcal{P}} \prod_{i<j}^{N} (z_i - z_j)^2 e^{-|z_i|^2/4l_0^2} det(e^{i\vec{k}\cdot\vec{r}}) \tag{4.13}$$

where $\hat{\mathcal{P}}$ is the projection operator onto the LLL and $det(e^{i\vec{k}\cdot\vec{r}})$ is the Slater determinant of CF plane waves. This wavefunction has some following important properties. The determinant renders the states totally antisymmetry, and the projection operator ensures they are entirely in LLL. Moreover, when comparing the pair distribution function obtained for exact ground state of 9 particles on a sphere at the LLL with that of the above trial state (4.13), Rezayi et al. found that these pair distribution functions are indistinguishable.

4.3 The quantum nematic state of the 2DEG at half-filled LL

In this section, we will discuss about the quantum nematic state proposed by Fradkin and Kivelson in [6]. In this paper, they introduced the quantum liquid crystalline phases which are analogy of the classical liquid crystal phases. Since the main focus of our work is the nematic phase so it is neccessary to introduce about the classical nematic phase. For a complete description of the classical nematic phase and other classical liquid-crystalline phases, one could refer to [44].

A nematic liquid crystal consists of series of rod-like molecules in a liquid. Each molecule in nematic phase is polarized (rod-like structure) so the nematic phase breaks rotational symmetry. Eventhough the directions of the polarization of the molecules are random they tend to point along a preffered direction which is called director of the nematic phase. In Fig. 4.3, we sketch a pictorial representation of a classical nematic phase.

One can define the order parameter that will pick out nematic order as follows:

$$Q = \int d^3\vec{r} d\theta n(\vec{r}, \theta)(3cos^2\theta - 1)/2 \tag{4.14}$$

where $n(\vec{r}, \theta)$ is the probability that a particle at $\vec{r}$ points along θ.

Figure 4.3: Schematic view of a classical nematic phase. Rod presents a polarized molecule in the liquid. The preffered direction of the nematic phase is the director $\vec{n}$.

In the papers by Kulakov et al. [45,46] and Folger et al. [47], it was shown that there exists a stripe ordered or charge density wave (CDW) for a 2 DEG at half-filled LL. According to their Hartree-Fock (HF) calculations, in this state, the electron density will exhibit periodic oscillation along a spatial direction. The electron in the partially filled LL will form stripes in which the LL is alternately full and empty. As such, the local Hall conductance is alternated between quantized values of $2Le^2/\hbar$ and $(2L+1)e^2/\hbar$ where L is the valence LL which is partially filled. Fradkin et al. [6] showed that the quantum mechanical fluctuation of this state can lead to a variety of new phases. They developed a phase diagram of electronic liquid crystalline phases which are quantum mechanical analogs of classical liquid crystals. These phases are classified based on symmetry breaking as follows:

- Quantum smectic phase, which has the CDW order. This phase breaks both the translational and rotational symmetries. It was argued in [6] that the stripe ordered state studied by HF approach in [45] is actually a smectic phase.

- Quantum nematic phase, in which quantum fluctuations of the stripe order are sufficiently strong restores the translational symmetry but breaks the rotational symmetry.

- Isotropic fluid phase, which has both the translational and rotational symmetry.

- Insulating stripe-crystal phase, which occurs when the partially valence LL is not half-filled. This phase is characterized by the same CDW order perpendicular to the stripe direction as the smectic, but in addition the density-wave fluctuations along neighboring stripes phase lock to each other, forming a true, insulating, two-dimensional electron crystal.

- Wigner crystal phase, which is also possible when the partial filling is close to 0 or 1. This phase is also insulating, but differs from the insulating stripe crystal in its crystal structure, and its degree of isotropy.

Fig. 4.4 taken from [48] shows some pictorial representation of stripes in the smectic phase, nematic phase, isotropic fuild phase and the crystal phase.

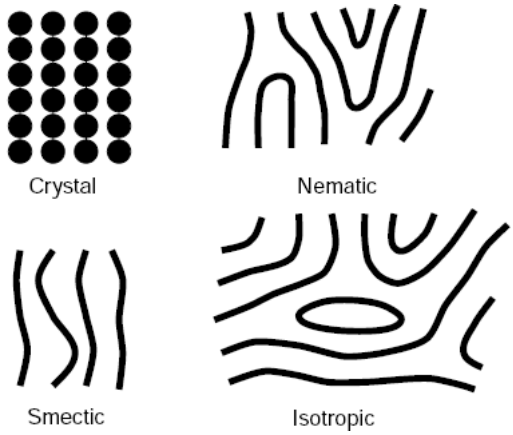

Figure 4.4: Schematic view of the quantum liquid-crystalline phases. Heavy lines respresent the stripes. One can view the nematic phase as melted smectic phase (two dislocations in the nematic phase are shown). In the crystal phase, the pinned CDW along the stripes are represented as filled circles.

Since the last two phases are only possible for a system with filling factor $\nu \neq 1/2$, we do not consider them for our half-filled system. On the other hand, both the smectic and the nematic phases break rotational symmetry. They possess highly anisotropic conductivity tensors which have the principle axes parallel to the "x direction" and perpendicular to the "y direction"-the preferred stripe orientational direction.

In [4, 49], the stripe ordered state is a anisotropic triangular Wigner crystal. In Fig. 7.2, we show some triangular Wigner crystal with different anisotropy parameter. The anisotropy paramter ε is defined via the lattice constants as:

$$a_1 = \sqrt{3}a/2\sqrt{1-\varepsilon}, \tag{4.15}$$

$$a_2 = \sqrt{1-\varepsilon}a/2. \tag{4.16}$$

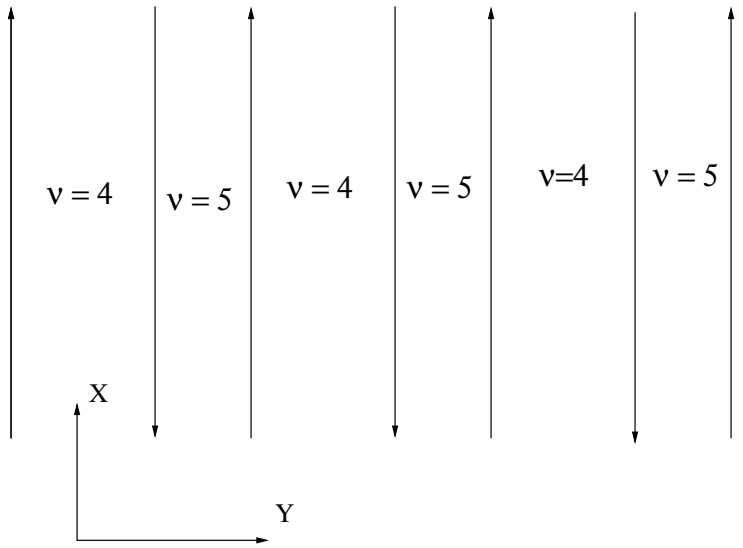

Figure 4.5: The schematic of the smectic phase for a filling factor between 9/2 and 4.

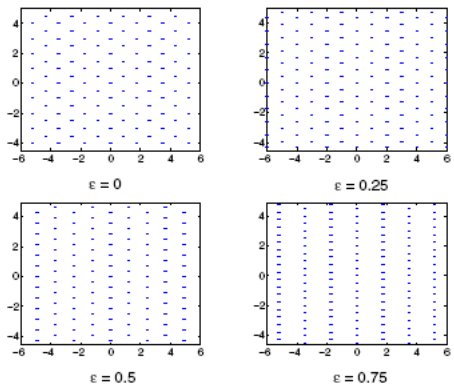

Figure 4.6: The anisotropic triangular WC lattice structure with various values of the uniaxal anisotropic parameter ε of the lattice.

For $\varepsilon = 0$, one has the isotropic WC crystal. For $\varepsilon > 0$, one has the stripe-ordered state. However, as one can see from Fig. 7.2, the higher the anisotropic paramter *varepsilon*, the clear the stripe ordered structure the lattices become.

It is natural to consider a finite temperature nematic state. A small anisotropy in the heterojunction device is a symmetry-breaking field that picks a preferred orientation for the

nematic state. This proposal was confirmed again in the paper done by Fradkin et al. [7]. In this paper, the authors carried out a classical MC simulation of nematic phase of 2DEG in a symmetry breaking field. The classical Hamiltonian of the system is given by:

$$H = -J \sum_{\vec{r},\mu=x,y} cos(2\Delta_\mu \theta_{\vec{r}}) + h \sum_{\vec{r}} cos(2\theta_{\vec{r}}), \tag{4.17}$$

where $\vec{r}$ is the lattice vectors of a square lattice of unit spacing. $\Delta_\mu \theta_{\vec{r}} = \theta_{\vec{r}+\vec{e}_\mu} - \theta_{\vec{r}}$ where $\vec{e}_\mu$ is a unit vector along direction $\mu = x, y$. J is the stiffness which is the energy required to rotate two nearby regions by a small angle. h represents the effect of the rotational symmetry breaking field which is anisotropy and/or effects of a parallel magnetic field. Fradkin et al. [7] presented an analysis of experimental data of Lilly et al. [2], and obtained a good theoretical fit as shown in the Fig. 4.7 (taken from [7]).

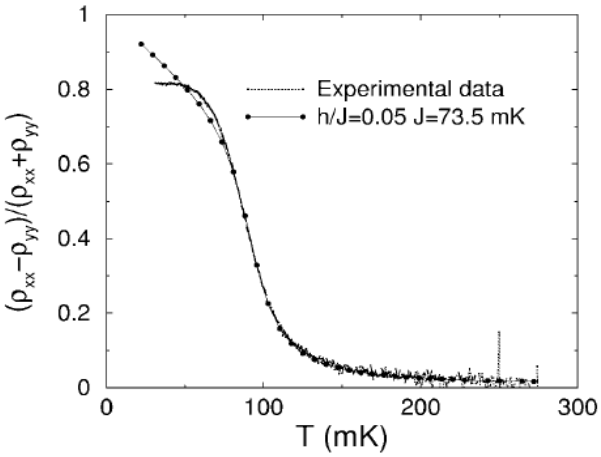

Figure 4.7: Fit of MC data for a 100×100 lattice to the experimental data [2]. The best fit found is for $J = 73mK, h = 0.05j = 3.5mK$ and $T_c = 65mK$, J and h are defined in equation (4.17).

Oganesyan et al. in [15] developed a microscopic theory of a electronic nematic fluid in two dimensions. In their approach the zero-temperature isotropic to nematic transition is the instability of the Fermi surface. The Fermi surface in the nematic phase will have an elliptical instead of a circular shape in the isotropic phase. In this state, the particle has different wave vectors along x and y so it breaks the rotational symmetry. In this paper,

they proposed a trial ground state wavefunction of the nematic state as follows:

$$\psi = \hat{P} \prod_{i<j} (z_i - z_j)^2 e^{-\sum_j |z_j|^2/2} Det[e^{i\vec{k}\cdot\vec{r}}] \tag{4.18}$$

where $Det[e^{i\vec{k}\cdot\vec{r}}]$ is the Slater determinant of a nematic wavefunction corresponding to an elliptical Fermi sea. This wavefunction is our ansatz wavefunction to study the nematic phase of 2DEG at half- filled LL.

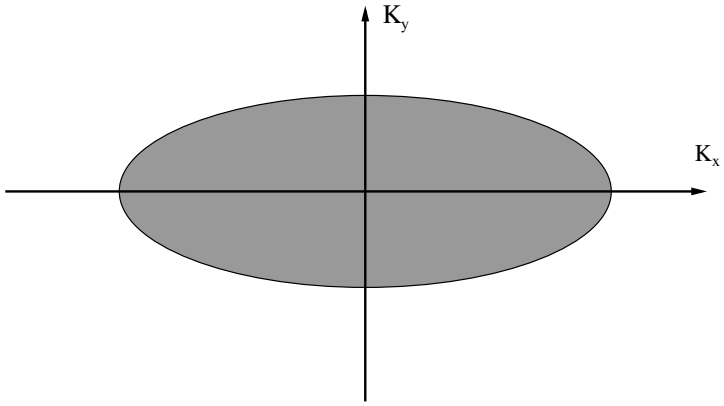

Figure 4.8: The Fermi surface of the nematic phase where $k_x \neq k_y$. Meanwhile, for the isotropic phase $k_x = k_y$.

CHAPTER 5

Variational FHNC study of the nematic state of half-filled LL system

The FHNC formalism for Fermi systems was introduced and developed in Refs. [50, 51]. A significant advantage of FHNC over the variational Monte Carlo is that FHNC does not suffer from finite-size effects. In the current problem, where we need to estimate small energy differences, the role of finite-size effects may be significant. The main idea of this method is to expand the pair distribution function in powers of the density of the system and it works well for a low-density system. The variational Monte Carlo becomes advantageous at relatively high density, as in the case of liquid ^{3}He, where the roles of the elementary diagrams and other nontrivial many-body correlations need to be included [52].

5.1 FHNC Formalism for the nematic state of half-filled LL system

In order to apply the FHNC formalism, first we assume that the unprojected wave function is a good approximation to the real wave function for the lowest Landau level (LLL). Moreover, it is known [17] that the projection operator almost eliminates the high LL components of the wave function. The potential energy of the high LL can be expressed [14] via the pair distribution function of the LLL using the single mode approximation discussed in Ref. [53], namely,

$$V_L = \frac{\rho}{2} \int \Big[g(\vec{r}) - 1 \Big] V^L_{eff}(r) d^2r \tag{5.1}$$

where the effective potential $V^L_{eff}(r)$ Landau level L is the convolution of the effective interaction [16] $V(r) = e^2/\epsilon\sqrt{r^2+\lambda^2}$ with the L-order Laguerre polynomials; namely, it

is the Fourier transform of:

$$\tilde{V}^{L}_{eff}(q) = \frac{2\pi e^2}{\epsilon q} e^{-\lambda q} \left[L_L(q^2/2) \right]^2 \tag{5.2}$$

In the above formula, λ is a length scale which characterizes the confinement of the electron wave function in the direction perpendicular to the heterojunction [16].

Our calculation proceeds as follows: First, we will calculate the pair distribution functions for isotropic and nematic states with different values of the anisotropic parameter for the LLL using the FHNC approximation. Second, the interaction energies will be calculated via the pair distribution functions by using the single-LL approximation, i.e., via Eq. (5.1). Next, the kinetic energy is evaluated for the isotropic and different nematic states. The energy values of the isotropic state are compared with anisotropic states for the lowest, first, and second excited LLs to find out if the nematic state becomes energetically favorable. Finally, we will carry out a self-consistent Hartree-Fock calculation [4, 49] for the more general case where λ can be nonzero and we will compare the energies of the nematic, isotropic, and stripe ordered Wigner crystals.

In the FHNC technique, each term in the expansion of the pair distribution function is represented as graphical diagrams with well-defined topological rules. There are nodal, composite, and elementary diagrams. The pair distribution function can be written in terms of these diagrams as follows:

$$g(\vec{r}_{12}) = 1 + X_{dd}(\vec{r}_{12}) + N_{dd}(\vec{r}_{12}) + 2\left[X_{de}(\vec{r}_{12}) + N_{de}(\vec{r}_{12}) \right] + X_{ee}(\vec{r}_{12}) + N_{ee}(\vec{r}_{12}) \tag{5.3}$$

In the above equation:

- $g(\vec{r}_{12})$ is the pair distribution function,
- $N_{dd}(\vec{r}_{12}), N_{de}(\vec{r}_{12}), N_{ee}(\vec{r}_{12})$ are the dd, de and ee nodal diagrams,
- $X_{dd}(\vec{r}_{12}), X_{de}(\vec{r}_{12}), X_{ee}(\vec{r}_{12})$ are the dd, de and ee composite diagrams.

In the FHNC/0 approximation, which neglects the elementary diagrams, the pair distribution function is obtained by solving the FHNC integral equations given in Ref. [52] for the case of polarized liquid ^{3}He. Thus, the equations of sum of nodal diagrams are given

as follows:

$$X_{dd}(\vec{r}_{12}) = e^{u(\vec{r}_{12})+N_{dd}(\vec{r}_{12})} - N_{dd}(\vec{r}_{12}) - 1, \tag{5.4}$$

$$X_{de}(\vec{r}_{12}) = e^{u(\vec{r}_{12})+N_{dd}(\vec{r}_{12})} N_{de}(\vec{r}_{12}) - N_{de}(\vec{r}_{12}), \tag{5.5}$$

$$X_{ee}(\vec{r}_{12}) = e^{u(\vec{r}_{12})+N_{dd}(\vec{r}_{12})} \Bigg[N_{ee}(\vec{r}_{12}) + |N_{de}(\vec{r}_{12})|^2 - g_s |N_{cc}(\vec{r}_{12}) - l(\vec{r}_{12})|^2 \Bigg] - N_{ee}(\vec{r}_{12}), \tag{5.6}$$

$$X_{cc}(\vec{r}_{12}) = e^{u(\vec{r}_{12})+N_{dd}(\vec{r}_{12})} \Big[N_{cc}(\vec{r}_{12}) - l(\vec{r}_{12}) \Big] + l(\vec{r}_{12})/g_s - N_{cc}(\vec{r}_{12}) \tag{5.7}$$

The convolution equations of the nodal diagrams are:

$$N_{dd}(\vec{r}_{12}) = \rho \int d\vec{r}_3 \Big[X_{dd}(\vec{r}_{13}) + N_{dd}(\vec{r}_{13}) \Big] P(\vec{r}_{32}), \tag{5.8}$$

$$N_{de} = \rho \int d\vec{r}_3 \Big\{ X_{dd}(\vec{r}_{13}) X_{ee}(\vec{r}_{32}) - X_{de}(\vec{r}_{13}) X_{de}(\vec{r}_{32}) + \Big[X_{de}(\vec{r}_{13}) + N_{de}(\vec{r}_{13}) \Big] P(\vec{r}_{32}) \Big\}, \tag{5.9}$$

$$N_{ee}(\vec{r}_{12}) = \rho \int d\vec{r}_3 \Big\{ X_{de}(\vec{r}_{13}) X_{de}(\vec{r}_{32}) - X_{dd}(\vec{r}_{13}) X_{ee}(\vec{r}_{32}) + \Big[X_{ee}(\vec{r}_{13}) + N_{ee}(\vec{r}_{13}) \Big] P(\vec{r}_{32}) \Big\}, \tag{5.10}$$

$$N_{cc}(\vec{r}_{12}) = \rho \int d\vec{r}_3 \Big[- l(\vec{r}_{13})/g_s + X_{cc}(\vec{r}_{13}) + N_{cc}(\vec{r}_{13}) \Big] X_{cc}(\vec{r}_{32}) \tag{5.11}$$

where

$$P(\vec{r}_{ij}) = X_{dd}(\vec{r}_{ij}) + 2X_{de}(\vec{r}_{ij}) + \rho \int d\vec{r}_k \Big[X_{dd}(\vec{r}_{ik}) X_{ee}(\vec{r}_{kj}) - X_{de}(\vec{r}_{ik}) X_{de}(\vec{r}_{kj}) \Big]. \tag{5.12}$$

The pseudo-potential $u(r)$ for half-filled system is given by:

$$u(r) = 4ln(r) \tag{5.13}$$

$l(r_{12})$ is the statistical exchange factor for 2D Slater determinant and is given by:

$$l(\vec{r}_1, \vec{r}_2) = 2\frac{J_1(k_F r_{12})}{k_F r_{12}}, \tag{5.14}$$

with $r_{12} = |\vec{r}_1 - \vec{r}_2|$, $J_1(r)$ is the first order Bessel function and k_F is the Fermi momentum of the isotropic state. Alternatively, for the anisotropic state having an elliptic Fermi surface

with major and minor axes k_1 and k_2, we find:

$$l(\vec{r}) = 2\frac{J_1\left(\sqrt{(k_1x)^2 + (k_2y)^2}\right)}{\sqrt{(k_1x)^2 + (k_2y)^2}}, \tag{5.15}$$

where x and y are the coordinates of $\vec{r}$.

Since the potential $u(r)$ has the long-range logarithmic form, we follow the standard procedure used in [34, 54] to seperate it into long-range and short-range part as:

$$u(\vec{r}_{12}) = u_s(\vec{r}_{12}) + u_l(\vec{r}_{12}), \tag{5.16}$$

$$u_s(\vec{r}_{12}) = -4K_0(Qr_{12}), \tag{5.17}$$

$$u_l(\vec{r}_{12}) = 4ln(r_{12}) + 4K_0(Qr_{12}), \tag{5.18}$$

where $K_0(x)$ is the modified Bessel function and Q is a wave vector which introduces a short-wavelength cutoff. The 2D Fourier transform of $u_l(r)$ is given by:

$$\tilde{u}_l(\vec{q}) = -\frac{8\pi Q^2}{q^2(q^2 + Q^2)}. \tag{5.19}$$

Only the *dd*-type nodal and composite functions need to be split into a short- and a long-range part:

$$N_{dd}(\vec{r}_{12}) = N_{dds}(\vec{r}_{12}) - u_l(\vec{r}_{12}), \tag{5.20}$$

$$X_{dd}(\vec{r}_{12}) = X_{dds}(\vec{r}_{12}) + u_l(\vec{r}_{12}). \tag{5.21}$$

The splitting is done subjected to the following conditions:

$$u(\vec{r}_{12}) + N_{dd}(\vec{r}_{12}) = u_s(\vec{r}_{12}) + N_{dds}(\vec{r}_{12}), \tag{5.22}$$

$$N_{dd}(\vec{r}_{12}) + X_{dd}(\vec{r}_{12}) = N_{dds}(\vec{r}_{12}) + X_{dds}(\vec{r}_{12}). \tag{5.23}$$

This leads to a new set of FHNC equations for the short-range nodal and composite functions,

$$X_{dds}(\vec{r}_{12}) = e^{u_s(\vec{r}_{12}) + N_{dds}(\vec{r}_{12})} - 1, \tag{5.24}$$

$$X_{de}(\vec{r}_{12}) = e^{u_s(\vec{r}_{12}) + N_{dds}(\vec{r}_{12})} N_{de}(\vec{r}_{12}) - N_{de}(\vec{r}_{12}), \tag{5.25}$$

$$X_{ee}(\vec{r}_{12}) = e^{u_s(\vec{r}_{12}) + N_{dds}(\vec{r}_{12})} \Big[N_{ee}(\vec{r}_{12}) + |N_{de}(\vec{r}_{12})|^2 - g_s[N_{cc}(\vec{r}_{12}) - l(\vec{r}_{12})/g_s]^2 \Big] - N_{ee}(\vec{r}_{12}), \tag{5.26}$$

$$X_{cc}(\vec{r}_{12}) = e^{u_s(\vec{r}_{12}) + N_{dds}(\vec{r}_{12})} \Big[N_{cc}(\vec{r}_{12}) - l(\vec{r}_{12})/g_s \Big] + l(\vec{r}_{12})/g_s - N_{cc}(\vec{r}_{12}). \tag{5.27}$$

where g_s is the spin degree of freedom. Since we consider a system with spin-polarized then $g_s = 1$. From the convolution equations of nodal diagrams in real space, one can rewrite them in the momentum space and obtain:

$$\tilde{N}_{dds}(\vec{q}) = \frac{\rho\tilde{X}_{dds}(\vec{q})\tilde{P}(\vec{q}) + \tilde{u}_l(\vec{q})}{1-\rho\tilde{P}(\vec{q})}, \tag{5.28}$$

$$\tilde{N}_{de}(\vec{q}) = \frac{\rho\Big[\tilde{X}_{dd}(\vec{q})\tilde{X}_{ee}(\vec{q}) - \tilde{X}^2_{de}(\vec{q}) + \tilde{X}_{de}(\vec{q})\tilde{P}(\vec{q})\Big]}{1-\rho\tilde{P}(\vec{q})}, \tag{5.29}$$

$$\tilde{N}_{ee}(\vec{q}) = \frac{\rho\Big[\tilde{X}^2_{de}(\vec{q}) - \tilde{X}_{dd}(\vec{q})\tilde{X}_{ee}(\vec{q}) + \tilde{X}_{ee}(\vec{q})\tilde{P}(\vec{q})\Big]}{1-\rho\tilde{P}(\vec{q})}, \tag{5.30}$$

$$\tilde{N}_{cc}(\vec{q}) = \frac{\rho\Big[-\tilde{l}(\vec{q})/g_s + \tilde{X}_{cc}(\vec{q})\Big]}{1-\rho\tilde{X}_{cc}(\vec{q})}. \tag{5.31}$$

These equations (5.24)-(5.31) can be solved using the fixed-point iteration method. We set all nodal diagrams to 0 or values from previous iteration. Uisng Eqs. (5.24)-(5.31) we solve for nodal diagrams in momentum space. Then, one can invert-transform the nodal diagram functions from momentum space to real space. These values of nodal diagrams in real space can be used as the initial values for the next iteration. This process is repeated until self-convergence is achieved.

5.2 Results and discussions

We are interested in the potential- and total-energy difference between the isotropic ($\alpha = 1$) and the anisotropic case ($\alpha > 1$), namely,

$$\Delta V_L(\alpha,\lambda) = V_L(1,\lambda) - V_L(\alpha,\lambda), \tag{5.32}$$

$$\Delta E_L(\alpha,\lambda) = E_L(1,\lambda) - E_L(\alpha,\lambda), \tag{5.33}$$

as a function of λ and the anisotropy parameter α and for $L = 0$, $L = 1$, and $L = 2$. In the interesting region, the energy difference between the nematic and the isotropic state can be small relative to the energy scale e^2/l_0, so high accuracy may be required. The effective potential for high LL and for small values of λ changes rapidly at small distances and

oscillates at large distances. We have used an adaptive mesh to incorporate these multiscale oscillations accurately for up to $L = 2$. For higher Landau levels, it becomes increasingly more difficult to carry out an accurate calculation due to the fact that these oscillations become increasingly more rapid.

Our calculated pair distribution function for the isotropic state accurately reproduces the pair distribution function reported in Ref. [54] as illustrated in Fig. 5.1.

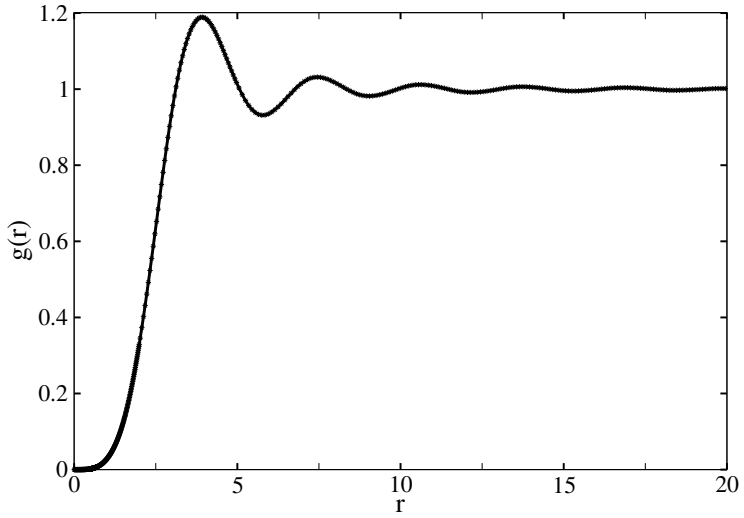

Figure 5.1: $g(r)$ vs. r for the isotropic state.

The potential-energy difference $\Delta V_L(\alpha, \lambda)$ for various values of α is calculated and shown in Figs. 5.2 and 5.3 in units of e^2/l_0 where $l_0 = \sqrt{hc/eB}$. Notice that for the case of the LLL and for the first excited LL, $\Delta V_L(\alpha, \lambda) < 0$, i.e., the isotropic state is energetically favorable for all values of λ and α. This is quite in agreement with the conclusion observed in the experiments [2].

However, as illustrated in Fig. 5.4, for the case of the second excited LL, $\Delta V_2(\alpha, \lambda) > 0$ for all values of α and for some range of the parameter λ, the anisotropic state can be energetically favorable provided that the energy loss due to the anisotropy of the Fermi surface is not larger than the potential-energy gain.

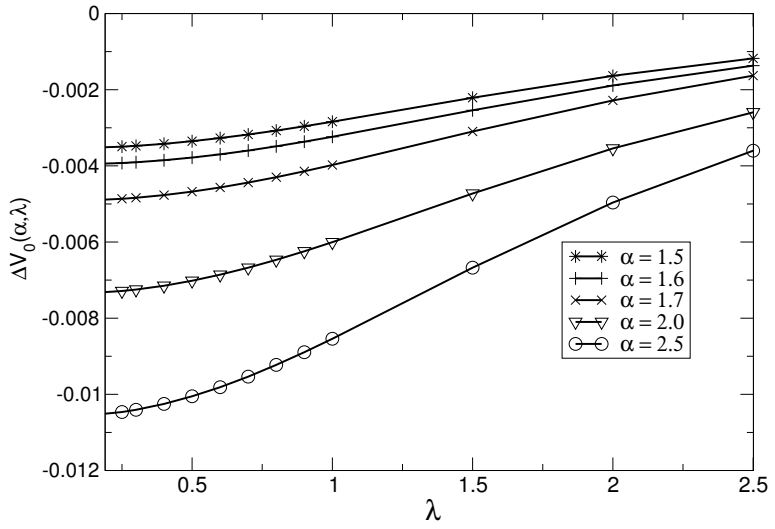

Figure 5.2: The potential energy difference $\Delta V_L(\alpha, \lambda)$ at the LLL as a function of λ for various values of the Fermi sea anisotropy parameter α.

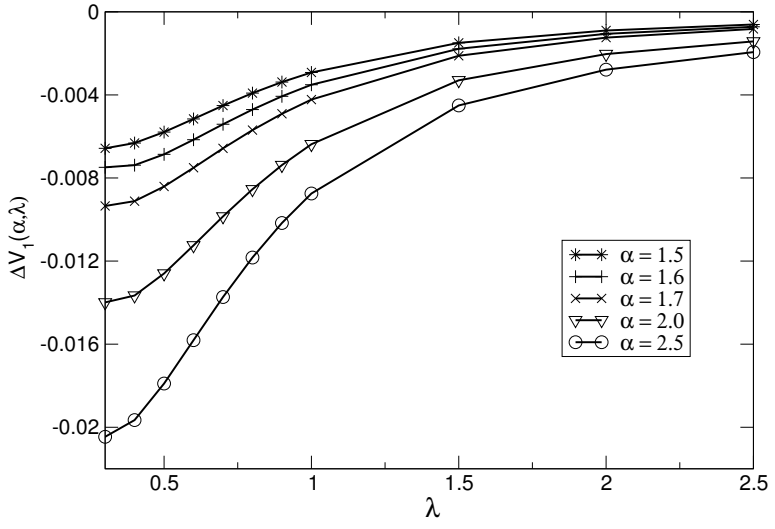

Figure 5.3: The potential energy difference $\Delta V_L(\alpha, \lambda)$ at the 1^{st} excited LLas a function of λ for various values of the Fermi sea anisotropy parameter α.

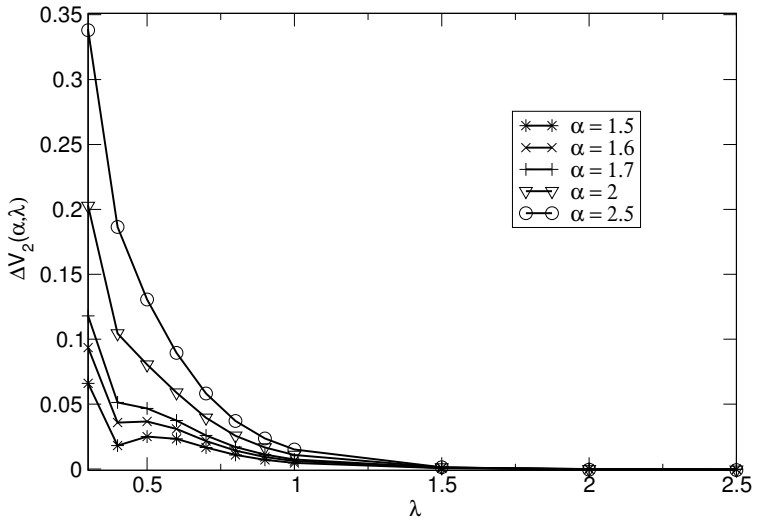

Figure 5.4: The potential energy difference $\Delta V_L(\alpha, \lambda)$ at the 2^{nd} excited LL as a function of λ for various values of the Fermi sea anisotropy parameter α.

In the single-LL approximation [53] the kinetic energy of the isotropic state is quenched. We can estimate the kinetic energy difference between the isotropic and the anisotropic case by ignoring the Landau-level projection operator and, thus, writing the wave function as $\Psi = F\Phi$, where Φ is the noninteracting Slater determinant and F the Jastrow part. The kinetic energy contains terms in which the operator $(\nabla - \vec{A})^2$ acts on F. This term gives the same contribution of $\hbar\omega_c/2$ in both isotropic and anisotropic cases. Therefore, the main difference, coming from the term $|F|^2\Phi^\star\nabla^2\Phi$, is due to the difference in shape of the Fermi sea. This leads to the following kinetic-energy difference between isotropic and anisotropic Fermi sea: $\Delta K \simeq -\frac{\hbar^2 k_F^2}{4m^\star}\frac{(1-\alpha)^2}{2\alpha}$ (see appendix A). In Fi.g 5.5, we present the total-energy difference $\Delta E_2(\alpha, \lambda)$ between the anisotropic and the isotropic state. Notice that the nematic state is energetically favorable relative to the isotropic below $\lambda_c \simeq 0.6$.

The results of Ref. [54] and ours share some qualitative similarities; Ciftja and Wexler found that while the ground state for the lowest LLL is isotropic, for the first and second excited LL, the anisotropic state becomes energetically favorable for a certain value of their

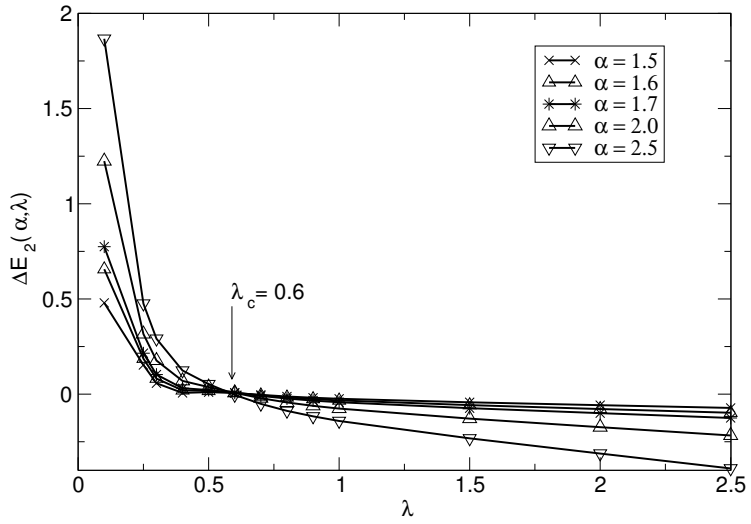

Figure 5.5: The total energy difference $\Delta E_L(\alpha, \lambda)$ at the 2^{nd} excited LL as a function of λ for various values of the Fermi sea anisotropy parameter α.

anisotropy parameter α. In contrast, in this thesis it is found that the isotropic state is still favorable for the first excited LL. This difference should be attributed to the difference between the two anisotropic wave functions: namely, the one used in our work has a symmetric Jastrow factor and an elliptical Fermi sea and is appropriate to model the nematic state [15], while the wave function used in Ref. [54] has an anisotropic Jastrow factor and a circular Fermi sea.

Hartree-Fock energies of the stripe and bubble charge density wave energy have already been reported [4, 49]; however, they are only available for the case of $\lambda = 0$. In order to compare the energy of the nematic state with that of the ordered stripe and the bubble states for a nonzero value of λ, we carried out a Hartree-Fock calculation using the method outlined in Refs. [4] and [49]. In Fig. 5.6, the total energy (apart from a common constant value of $\hbar\omega_c/2$) is compared with the results of our Hartree-Fock calculation for finite values of λ. In addition, in Fig. 5.7, the minimum energy with respect to the anisotropy parameter α is compared to the minimum Hartree-Fock energy value with respect to the uniaxial anisotropy parameter ε (the lattice constants of the uniaxial Wigner crystal are given in terms of as

$a_1 = \sqrt{3}a/2\sqrt{1-\varepsilon}$ and $a_2 = \sqrt{1-\varepsilon}a/2$). Notice that there is a critical value of λ, namely, $\lambda_c \simeq 0.4$, below which the nematic phase is energetically favored.

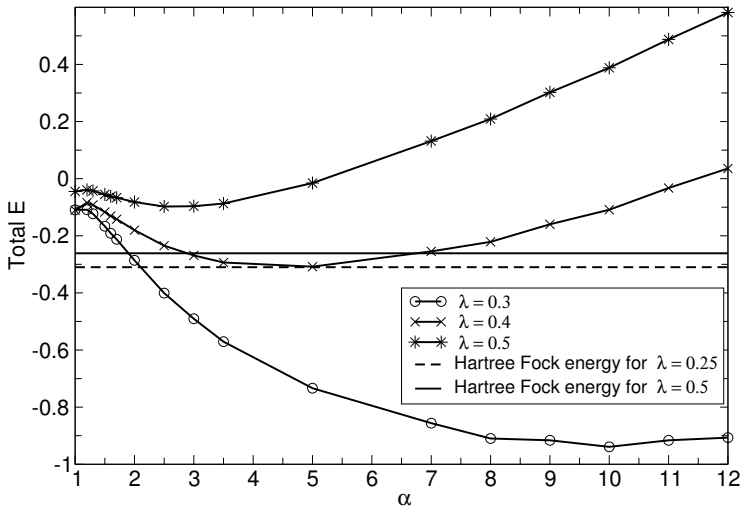

Figure 5.6: The total energy of the nematic state obtained by FHNC in comparison with stripe state obtained by HF

A value for the parameter λ can be estimated using the calculation presented in Ref. [16]. Using the value of the 2D electron density for these materials [2], we find that $\lambda \sim 62\mathring{A}$. This corresponds to a value of $\lambda \sim 0.34$ in units of the magnetic length l_0 ($l_0 = 181\mathring{A}$ for the value of $B \sim 2T$, which corresponds to the second excited LL in the experiments of Refs. [3] and [2]). This value of λ is less than the critical value $\lambda_c \simeq 0.4$ below which the nematic phase is energetically favorable as compared to the stripe ordered phase (see Fig. 5.7). Therefore, we conclude that our FHNC/0 calculation suggests that for the case of the 2DEG in the heterojunctions used in Refs. [3] and [2] the quantum nematic state [6, 7, 15] may be energetically lower than the stripe ordered or bubble phases.

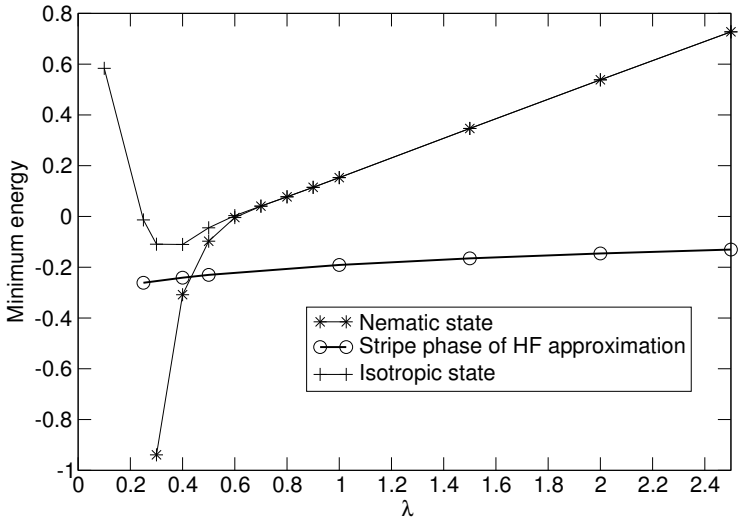

Figure 5.7: Optimal energy of nematic state obtained by FHNC in comparison with stripe state's optimal energy obtained by HF

There are two possible sources of systematic error in the present calculation. The first is the use of the FHNC/0 approximation to evaluate the distribution function, where the contribution of the elementary diagrams is neglected. This approximation works very well in low-density systems, i.e., where the average interparticle distance is large compared to a hard-core diameter. In the present problem, such a condition is not clearly fulfilled as there is only a soft core of size λ. The second source of error is the fact that we have neglected the projection operator and assumed that the unprojected wave function given by Eq. (5.1) is a good approximation to the lowest LL. In order to address these concerns, in Fig. 5.8 we compare only the potential energy of the nematic and isotropic states with the results of the Hartree-Fock approximation obtained for the same values of λ. Notice that for values of $\lambda > 0.6$, the results of the FHNC and the Hartree-Fock (HF) calculation are almost identical. Moreover, the results of the FHNC calculation for the isotropic state agree very well with those of the HF calculation for all values of $\lambda > 0.3$. This is an indication that the energy difference between the nematic phase and that of the isotropic state and the stripe state below $\lambda \simeq 0.5$ may not be an artifact of the difference in the treatment of the two states

(i.e., the difference between HF and FHNC approximations) but rather due to the fact that the nematic state for long-range interactions is energetically favorable for at least the second excited LL.

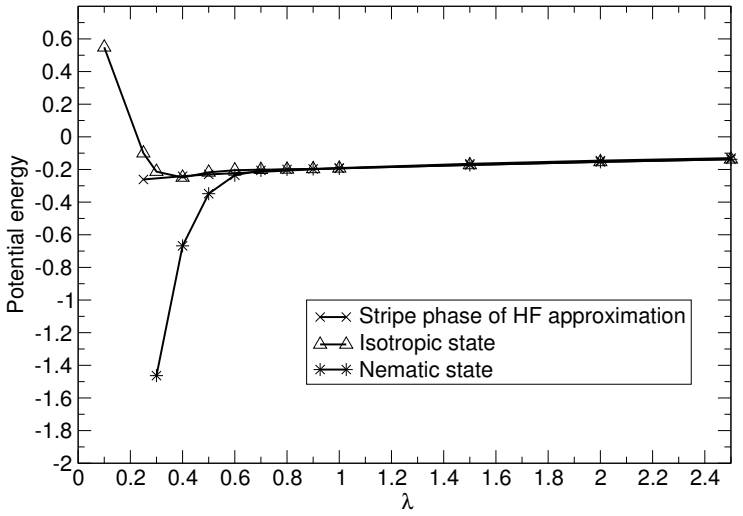

Figure 5.8: The potential energy at the optimal energy of the nematic state in comparison with the stripe state

CHAPTER 6

MC study of the nematic state of half-filled LL system

As mentioned previously, the FHNC works well for low density systems. In the FHNC approximation, the contribution of the elementary diagrams is ignored. To assess that the results obtained by FHNC are reliable, one needs to compare with other reliable methods. In this chapter, we will discuss the MC approach which is used to study the nematic state and we will compare the results with those obtained by FHNC. With MC, one is not subjected to the low density restriction which hinders FHNC. On the other hand, one needs to be concerned about the finite size effects. In other words, one will have difficulty in extrapolating the results to the thermodynamic limit. However as we will show, for large enough system size (of more than 100 particles) the results for the energy seem not to change significantly with the size of the system, so we will compare with the results obtained for systems with 100 particles or more.

The geometry we use is a square with periodic boundary conditions. This geometry has the advantage of naturally adapting to the nematic state wavefunction. There are several steps in applying the MC approach for this problem. First, for this wavefunction one needs to construct the Slater determinant of plane waves of states confined in an elliptical Fermi sea. Second, since the Coulomb interaction in 2D is $ln(r)$, which is a long-range interaction, to carry out the pseudo-potential computation one has to take into account all periodic image charge interactions. One of the methods to do this is the Ewald summation technique.

In the next section, we will describe the Ewald summation technique. In section 6.2 we will discuss how we implement the MC to study the nematic state. In section 6.3 we will discuss the results and comparison with FHNC.

6.1 Ewald summation technique for the logarithmic potential

We have already shown how the Ewald summation technique is applied for the case of 1/3 FQHE system in chapter 2. However, as discussed in the implementation of the FHNC calculation (see appendix C), the effective interaction for the 2^{nd} excited LL has a highly oscillatory behavior at small r and approaches zero very slowly at large r, so we need to derive the formalism for the Ewald sum of all image charge interactions which captures both small r and large r behavior.

The summation of the $ln(r)$ potential for periodic 2D systems is also developed by Jensen [55] and Lekner [56]. Their recipes were outlined in detail in [55], [56]. To have a better judgment of our Ewald summation technique, we want to compare its results with the results obtained from Jensen's method and find out for our particular problem whether they are the same.

The idea of Ewald summation is to add around each charge an opposite Gaussian charge distribution of an appropriately chosen width μ, and, in addition, to subtract the same Gaussian charge distribution. Let the density ρ_1 correspond to the charge combination of the particle together with the opposite Gaussian charge distribution and let ϕ_1 be the corresponding potential. ϕ_1 is a short-range potential, and, thus, we can calculate ϕ_1 in real space since it converges very quickly. The other combined charge configuration, consisting of the Gaussian and the background charge, is denoted by ρ_2 and the corresponding potential is denoted by ϕ_2. Since ϕ_2 is a long-range potential it will be summed in Fourier space. By adjusting the width parameter, μ, appropriately, we can make both sums converge very fast. Of course, the final result does not depend on μ.

Specifically, the original charge distribution is given as:

$$\rho(\vec{r}) = \sum_{\vec{R}} \delta(\vec{r} - \vec{R}) + \rho_{background} \tag{6.1}$$

The general 2D Poisson equation for this charge configuration is given by:

$$\nabla^2 \Phi(\vec{r}) = -2\pi\rho(\vec{r}) \tag{6.2}$$

Let us split ρ into long-range and short-range portions in the following manner:

$$\rho(\vec{r}) = \rho_1(\vec{r}) + \rho_2(\vec{r}) \tag{6.3}$$

$$\rho_1(\vec{r}) = \sum_{\vec{R}} \frac{e^{-\frac{(\vec{r}-\vec{R})^2}{\mu^2}}}{\pi\mu^2} + \rho_{background} \tag{6.4}$$

$$\rho_2(\vec{r}) = \sum_{\vec{R}} \left[\delta(\vec{r}-\vec{R}) - \frac{e^{-\frac{(\vec{r}-\vec{R})^2}{\mu^2}}}{\pi\mu^2}\right] \tag{6.5}$$

Now consider the potential ϕ_2. We can start with:

$$\nabla^2\phi = -2\pi\rho \tag{6.6}$$

$$\rho(\vec{r}) = \frac{1}{\pi\mu^2}e^{-r^2/\mu^2} \tag{6.7}$$

$$\vec{E} = -\vec{\nabla}\phi(\vec{r}) \tag{6.8}$$

$$\vec{\nabla}\cdot\vec{E} = 2\pi\rho(\vec{r}) \tag{6.9}$$

$$\tag{6.10}$$

Integrating E around the charge, one can obtain:

$$E(r) = \frac{1-e^{-r^2/\mu^2}}{r} \tag{6.11}$$

Then

$$\phi(r) = -\int_{r_0}^{r} E dr' \tag{6.12}$$

$$\phi(r) = -ln(r/r_0) + \int_{r_0}^{r} \frac{-e^{-r'^2/\mu^2}}{r'} dr \tag{6.13}$$

One can calculate the integral:

$$I = \int_{r_0}^{r} \frac{-e^{-r'^2/\mu^2}}{r'} dr' \tag{6.14}$$

and easily obtain:

$$I = \frac{1}{2}Ei(t) + const, \tag{6.15}$$

where $Ei(t)$ is the Exponential integral function and is defined by: $Ei(t) = -\int_{-t}^{\infty} \frac{e^{-x}}{x} dx$.
So the expression of I is given by:

$$I = \frac{1}{2}Ei\left(-\frac{r^2}{\mu^2}\right) + const \tag{6.16}$$

Thus, for:

$$\rho_2(\vec{r}) = \sum_{\vec{R}} \left[\delta(\vec{r} - \vec{R}) - \frac{e^{-(\vec{r}-\vec{R})^2/\mu^2}}{\pi\mu^2} \right], \tag{6.17}$$

the corresponding potential $\phi_2(r)$ is:

$$\phi_2(r) = -\frac{1}{2} \sum_{\vec{R}} Ei\left(- \frac{(\vec{r} - \vec{R})^2)}{\mu^2} \right) + const. \tag{6.18}$$

For the case of $\phi_1(r)$ which is periodic we expand both ρ_1 and ϕ_1 in terms of $\phi_{\vec{k}}(\vec{r}) = \frac{1}{\sqrt{A}} e^{i\vec{k}\cdot\vec{r}}$, where $\vec{k}$ is such that:

$$e^{i\vec{k}\cdot(\vec{r}+\hat{x}L)} = e^{i\vec{k}\cdot\vec{r}} \tag{6.19}$$

$$e^{i\vec{k}\cdot(\vec{r}+\hat{y}L)} = e^{i\vec{k}\cdot\vec{r}}, \tag{6.20}$$

where the size of the periodic box is $L \times L$. Therefore, we find that:

$$k_x L = 2\pi n_x, k_y L = 2\pi n_y \quad n_{x,y} = 0, \pm 1, \pm 2, \ldots \tag{6.21}$$

i.e

$$\vec{k} = \frac{2\pi}{L}\vec{n}, \tag{6.22}$$

where $\vec{n} \in Z^2$.

Thus, we can write:

$$\phi_1(\vec{r}) = \frac{1}{\sqrt{A}} \sum_{\vec{k}} \tilde{\phi_1}(\vec{k}) e^{i\vec{k}\cdot\vec{r}}, \tag{6.23}$$

where

$$\tilde{\phi_1}(\vec{k}) = \frac{1}{\sqrt{A}} \int_A d^2 r e^{-i\vec{k}\cdot\vec{r}} \phi_1(\vec{r}). \tag{6.24}$$

Using this basis:

$$\rho_1(\vec{r}) = \frac{1}{\sqrt{A}} \sum_{\vec{k}} \tilde{\rho_1}(\vec{k}) e^{i\vec{k}\cdot\vec{r}} \tag{6.25}$$

$$\tilde{\rho_1}(\vec{k}) = \frac{1}{\sqrt{A}} \frac{1}{\pi\mu^2} \int_A d^2 r e^{-i\vec{k}\cdot\vec{r}} e^{-\frac{r^2}{\mu^2}} \tag{6.26}$$

here we have assumed that $\rho_1(\vec{r}) = 0$ for $r > \frac{L}{2}$, i.e $\mu \ll \frac{L}{2}$. By carrying out the integral one can obtain:

$$\tilde{\rho_1}(\vec{k}) = \frac{1}{\sqrt{A}} e^{-\frac{\mu^2 k^2}{4}}. \tag{6.27}$$

$$\tag{6.28}$$

Again we have assumed that $L/\mu \gg 1$ (i.e $A \to \infty$).
Therefore, the equation $\nabla^2 \phi_1(\vec{r}) = -2\pi\rho_1(\vec{r})$ becomes:

$$-k^2 \tilde{\phi_1}(\vec{k}) = -2\pi\tilde{\rho_1}(\vec{k}), \tag{6.29}$$

and, hence,

$$\phi_1(\vec{r}) = 2\pi \frac{1}{A} \sum_{\vec{k}\neq 0} \frac{1}{k^2} e^{-\frac{\mu^2 k^2}{4}} e^{i\vec{k}\cdot\vec{r}}, \tag{6.30}$$

where $\vec{k} = \frac{2\pi}{L}\vec{n}$, $\vec{n} \in Z^2$.
Finally, if we note that for our case the charge of the particle is $e^2 = 2m$, then the original potential is the sum of potential ϕ_1 and ϕ_2 given as follows:

$$\phi_1(\vec{r}) = \frac{4m\pi}{A} \sum_{\vec{k}\neq 0} \frac{e^{-\mu^2 k^2/4}}{k^2} e^{i\vec{k}\cdot\vec{r}}, \tag{6.31}$$

$$\phi_2(\vec{r}) = -m \sum_{\vec{R}} Ei\left[-\frac{(\vec{r} - \vec{R})^2}{\mu^2} \right]. \tag{6.32}$$

Jensen in [55] carries out the summation of $u(r) = -ln(r)$ in a periodic 2D system and obtains:

$$V(x,y) = C + \pi\left(\frac{y}{L}\right)^2 - \frac{1}{2} ln\left[\prod_{k=-\infty}^{\infty} \frac{cosh(2\pi(y/L + k)) - cos2\pi x/L}{cosh2\pi k} \right], \tag{6.33}$$

where C is an integral constant and has the following form:

$$C = \frac{\pi}{6} - \frac{1}{2} ln2 - ln \prod_{k=1}^{\infty} \Big(1 + exp(-4\pi k)\Big). \tag{6.34}$$

For the Ewald summation, the convergence of (6.31) and (6.32) is achieved choosing the width of the Gaussian charge distribution $\mu = 1$, the number of cells for the sum in (6.32) to be 10 and by carrying out the sum in momentum space in (6.31) over 200 k-states. For the Lekner summation, the sum (6.33) converges within an accuracy of 10^{-5} just by using the following nine k values $k = -4 \ldots 4$. The difference between the two potentials is about 0.03%.

6.2 Procedure

Given a value of α there are discrete values of N (number of particles) which correspond to a closed shell. These discrete values of N are calculated as follows. The occupied states characterized by k_x, k_y must satisfy the following condition:

$$\left(\frac{k_x}{k_1}\right)^2 + \left(\frac{k_y}{k_2}\right)^2 \leq 1, \tag{6.35}$$

where k_1 and k_2 are the major and minor axis of the Fermi sea and given by:

$$k_1 = \sqrt{\frac{4\pi\rho}{\alpha}}, \tag{6.36}$$

$$k_2 = \sqrt{4\pi\rho\alpha}, \tag{6.37}$$

where ρ is the uniform particle density of the system. For a finite system of size $L \times L$, $k_x = n_x\Delta k$ and $k_y = n_y\Delta k$ where $\Delta k = 2\pi/L$ and $n_x, n_y \in Z$. So one can deduce the conditions for n_x, n_y such that:

$$\frac{\pi}{N}\left(\alpha n_x^2 + \frac{n_y^2}{\alpha}\right) \leq 1 \tag{6.38}$$

For a value of N to be acceptable the number pairs (n_x, n_y) satisfying the above inequality should be equal to N. For example, for $\alpha = 1$, N can be $1, 5, 9, 13, 21, 25, 29, 37, 45, \ldots$; for $\alpha = 2$, they can be $1, 3, 7, 11, 15, 17, 21, \ldots$

As one can see that with anisotropy parameter $\alpha = k_x/k_y > 1$, the occupied states (i.e those satisfying equation 6.38) are anisotropically distributed along the preferred k_x axis. In Figs. 6.1, 6.2 and 6.3 we present three examples of closed shell which correspond to $\alpha = 2, 3$ and 4. Our MC calculation will use these cases as well as larger size systems up to 145 particles. We follow the Metropolis MC scheme for sampling the wavefunction [57]. Initially, the positions

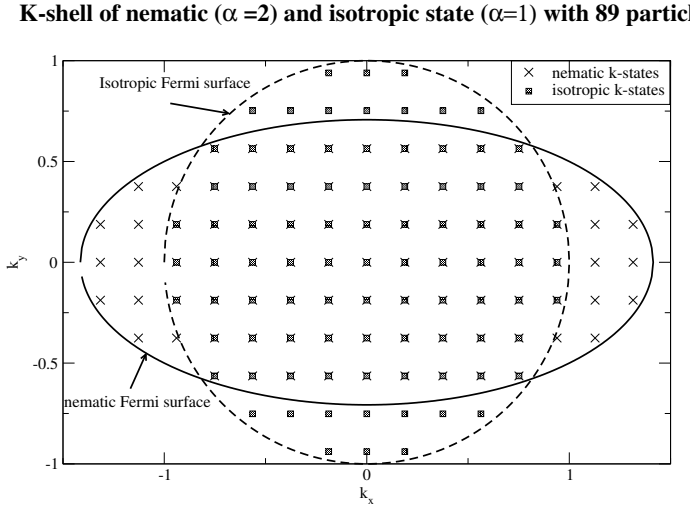

Figure 6.1: K-states for the nematic state with $\alpha = 2$

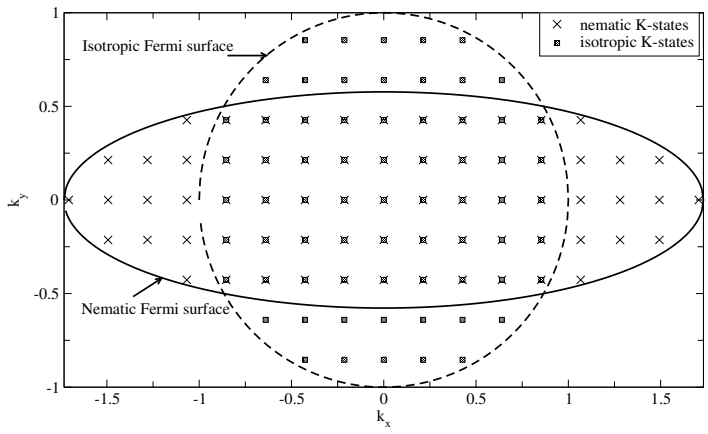

Figure 6.2: K-states for the nematic state with $\alpha = 3$

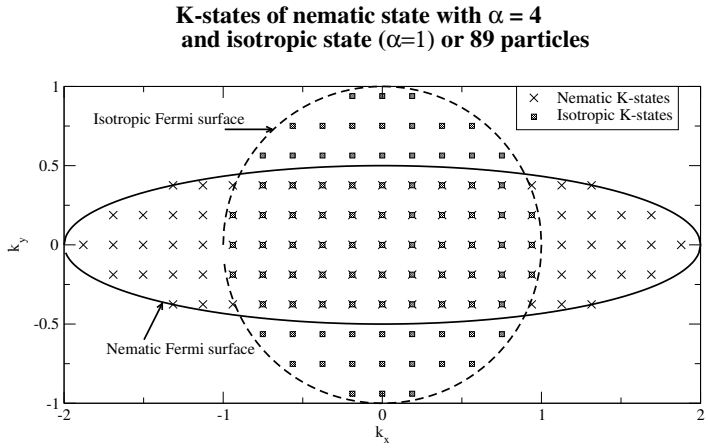

Figure 6.3: K-states for the nematic state with $\alpha = 4$

of the particles are populated randomly or from the previous MC step. A MC step consists of attempts to move all particles one by one to a trial positions as follows:

$$x_i^{new} = x_i^{old} + p_x\Delta, \tag{6.39}$$

$$y_i^{new} = y_i^{old} + p_y\Delta, \tag{6.40}$$

where p_x, p_y are random numbers sampled from uniform distribution between $(-1, 1)$ and Δ is an adjustable distance parameter.

The new position for particle i is accepted with a probability given by:

$$P = min\left[1, \left|\frac{\psi(\vec{r}_{new})}{\psi(\vec{r}_{old})}\right|^2\right] \tag{6.41}$$

where $\psi(\vec{r})$ is the unprojected wavefunction (4.18). The parameter Δ is adjusted so that the acceptance rate of the new configuration is about $30 - 50\%$.

Specifically, the ratio between the new and the old wavefunction is:

$$\left|\frac{\psi(\vec{r}_{new})}{\psi(\vec{r}_{old})}\right|^2 = exp(u(\vec{r}_{new}) - u(\vec{r}_{old}))\left|\frac{Det(e^{i\vec{k}\cdot\vec{r}_{new}})}{Det(e^{i\vec{k}\cdot\vec{r}_{old}})}\right| \tag{6.42}$$

where $u(\vec{r})$ is the periodic pseudo-potential which is derived in previous section.

To carry out the calculation of the ratio between the Slater determinant of the new configuration and the old configuration efficiently, we use the inverse updating technique developed by Ceperley et al. [58]. After one MC step, the particle configuration is used to calculate the value of physical quantities under consideration. Then, we average over these values for a large number of MC steps to obtain the desired expectation value. Note that, in the MC simulation, the error in the expectation value behaves as $1/\sqrt{N_{MCS}}$ where N_{MCS} is the number of MC steps. In addition, before averaging, one usually needs to reach "thermalization" by disregarding a number of initial configurations. More detailed discussion about the MC simulation can be found in [59]. For our problem, we found that the number of MC steps for "thermalization" is of the order of 10^5 and we use of the order of 2×10^6 MC steps to calculate averages of the distribution function.

Since we use the single LL approximation to calculate the interaction energy at high LL (equation 5.1), we are interested in obtaining the expectation value of the pair distribution function $g(\vec{r})$. Specifically, for each configuration, we compute the histogram of vectorial "distance" between any two particles which lie between (x, y) and $(x + dx, y + dy)$. This histogram obtained by averaging over N_{MCS} MC steps corresponds to the quantity $2g(x, y)\rho N_e N_{MCS} dxdy$. The pair distribution function obtained this way always satisfies the condition:

$$\rho \int d^2r[g(\vec{r}) - 1] = -1. \tag{6.43}$$

The approach can be divided into the following steps:

- we calculate the pair distribution function at the LLL for different anisotropic parameters α.
- we use the single LL approximation [53] to calculate the interaction energies at a high LL.
- next, the kinetic energies for different anisotropic parameters is evaluated (see appendix A).
- we compare total energies of the isotropic and nematic state to find out at what LL the nematic becomes more stable.

- we determine the value of α (optimum) which corresponds to the lowest energy.
- the optimum total energies of the nematic states will be compared with those of the stripe states at different values of λ at the excited 2^{nd} LL to find out at what values of λ the nematic state is energetically favorable.
- this critical value of λ will be compared with the values which correspond to those samples used in the experiment [2].
- the comparison of the results obtained by MC to the ones obtained by FHNC will also be presented.

6.3 Results and Discussion

First, we show that the pair distribution function, $g(r)$, obtained using MC, has important differences as compared to $g(r)$ obtained by FHNC, as illustrated in Fig. 6.4. Thus, it is important to obtain the energies of the nematic state at high LL by MC and to compare them with those obtained by FHNC.

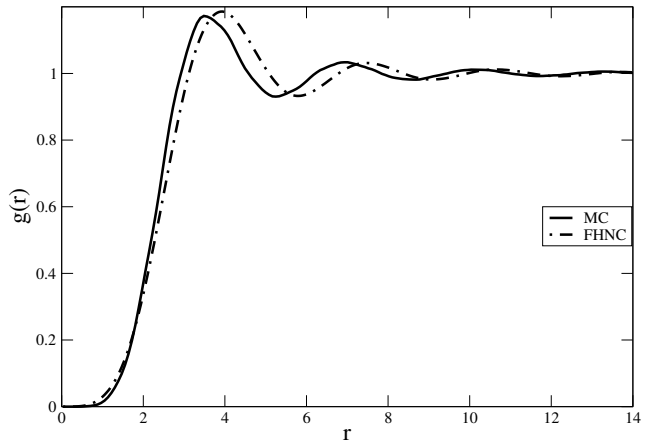

Figure 6.4: Comparison of the pair distribution function obtained by FHNC and MC.

We study the instability of the nematic state at the LLL and the 1^{st} excited LL by comparing the interaction energies obtained for different values of $\alpha > 1$ with those of the isotropic state ($\alpha = 1$) (Figs. 6.5 and 6.6).

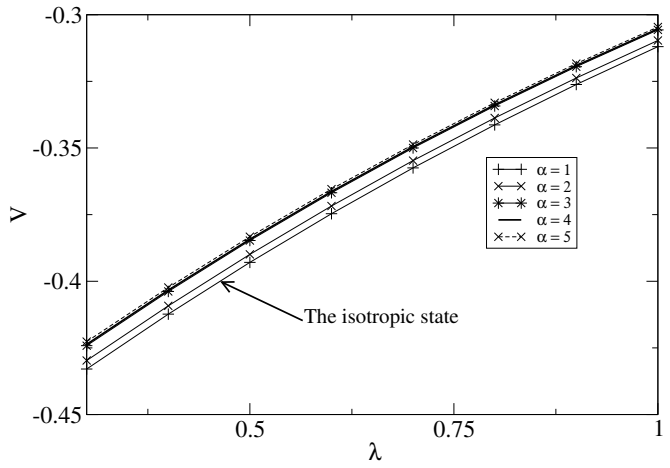

Figure 6.5: Comparison of the potential energy of the nematic state calculated for various values of $\alpha \neq 1$ as function of λ with the isotropic state ($\alpha = 1$) at LLL.

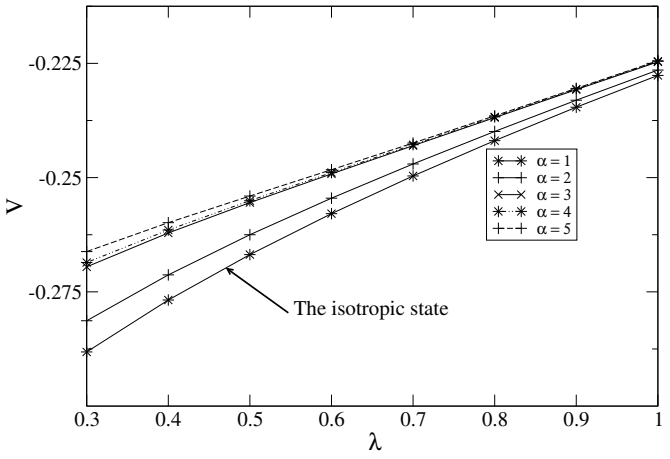

Figure 6.6: Comparison of the potential energy of the nematic state calculated for various values of $\alpha \neq 1$ as function of λ with the isotropic state ($\alpha = 1$) at the 1^{st} excited LL.

As one can see from Figs. 6.5 and 6.6, the interaction energy of the isotropic state is always lower than those of the nematic state for the 1^{st} excited LL and LLL. The potential energy is calculated with the pseudo-potential obtained using the Ewald sum. A similar result is also found with the pseudo-potential using the Lekner sum. On the other hand, as shown in appendix A, the kinetic energy of the isotropic state is below that of the nematic state, and, thus, the total energy of the isotropic state is always lower than that of the nematic state. Hence, our MC calculation shows that the isotropic state is always energetically favorable as compared to the nematic state at LLL and the 1^{st} excited LL. Also note that, in the previous chapter, using FHNC we also found that for LLL and the 1^{st} excited LL the isotropic state is energetically favorable as compared to the nematic state for all values of λ. These findings solidify the conclusion that at the LLL and the 1^{st} excited LL, the isotropic state is more stable than the nematic state, which is also in agreement with the experimental findings of Refs. [2] and [3].

However, at the 2^{nd} excited LL, the situation changes as illustrated in Fig. 6.7.

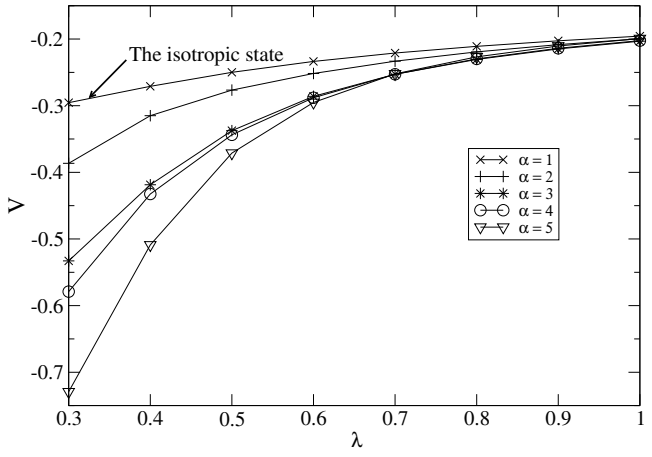

Figure 6.7: Comparison of the potential energy of the nematic state calculated for various values of the anisotropic parameter $\alpha \neq 1$ as function of λ with the isotropic state ($\alpha = 1$) at the 2^{nd} excited LL

As one can see from this figure, the interaction energy of the nematic state is now always lower than that of the isotropic state. Next, we compare the total energies for nematic state and the isotropic state at the 2^{nd} excited LL (Fig. 6.8) to find out at what value of λ the nematic state becomes energetically lower than the isotropic state.

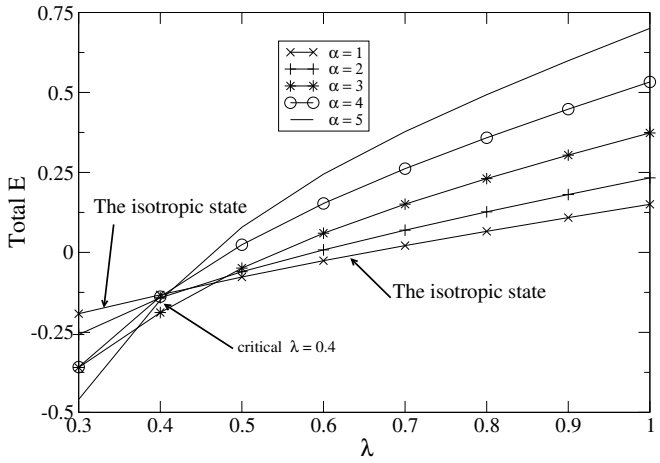

Figure 6.8: Comparison of total energy of the nematic state calculated for various values of the anisotropic parameter $\alpha \neq 1$ as functions of λ with the isotropic state ($\alpha = 1$) at the 2^{nd} excited LL

From Fig. 6.8, one can see that the nematic state is energetically favorable as compared to the isotropic state at the 2^{nd} excited LL for a range of values of $\lambda \leq 0.4$. Note that, using FHNC we found for $\lambda \leq 0.6$, the nematic state is more stable than the isotropic state. In short, both FHNC and MC yield similar conclusions about the stability of the nematic state versus the isotropic state at the 2^{nd} excited LL.

In [4], [5], [49], it was argued that the stripe-ordered phase can be a candidate to explain the anisotropy seen in the transport properties of the 2DEG at low temperature. Therefore, we also need to investigate the stability of the nematic state versus the stripe-ordered state as follows. First, we find the optimum energies of the nematic state with respect to the anisotropic parameter α at different values of λ. Next, we compare these with the optimum energies of the stripe state obtained by HF. Detailed HF calculations of the stripe state are shown in the next chapter. Remember that for the stripe-ordered state, the optimum energy

is obtained by minimizing the energy with respect to the uniaxial anisotropy parameter ε (see next chapter for the definition of ε). Calculations for the case where $\lambda = 0$ have been carried out in Refs. [4] and [5]. For the purpose of our work presented here, we need to extend these calculations for the case where $\lambda \neq 0$. Such calculation were not available in the literature. Fig. 6.9 shows the comparison of the optimal energies obtained by MC for the nematic state and the stripe state obtained by HF. Note that, for $\lambda \geq 0.5$, the optimum nematic state corresponds to the isotropic state ($\alpha = 1$).

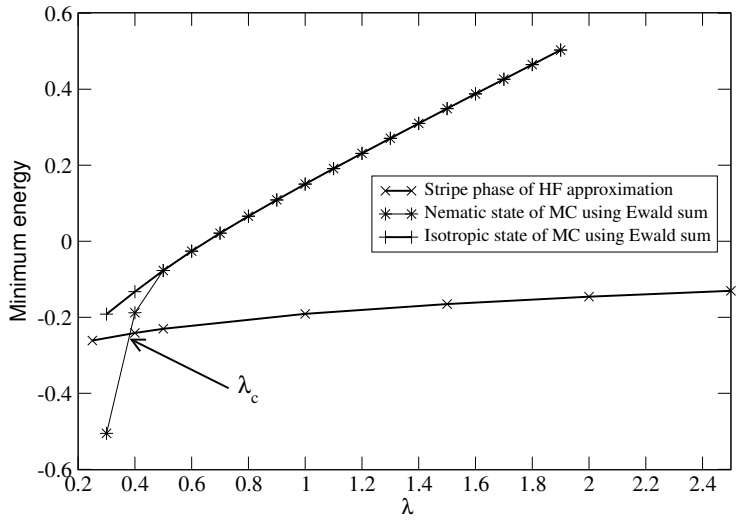

Figure 6.9: Comparison of the optimal nematic state calculated by MC using the pseudo-potential using the Ewald sum with the stripe state calculated by HF as function of λ

From Fig. 6.9, we can see that the nematic state is energetically lower than the stripe state for the values of $\lambda \leq \lambda_c = 0.37$. As discussed in section 6.1, the pseudo-potential can be obtained by using either the Ewald or the Lekner summation technique. The difference between two pseudo-potential is about 0.03%. The origin of this discrepancy is attributed to the fact the sums (6.31) and (6.32) of pseudo-potential obtained by Ewald summation were carried out with finite numbers of basic cell (with finite size) and reciprocal lattice cell. The same argument is applied for the case of Lekner summation (equation (6.33)). We believe

that if we make the mesh and the range of r finer and greater (by increasing the size of the basic cell), this difference can be removed. However, this requires computational time scales beyond our present capacity to handle. In addition, our conclusions are not affected by such small error. To demonstrate this, we also obtained the optimum energy for the nematic state in which the pseudo-potential obtained by the Lekner sum and compare this with the stripe state energy and results calculated by Ewald sum (Fig. 6.10).

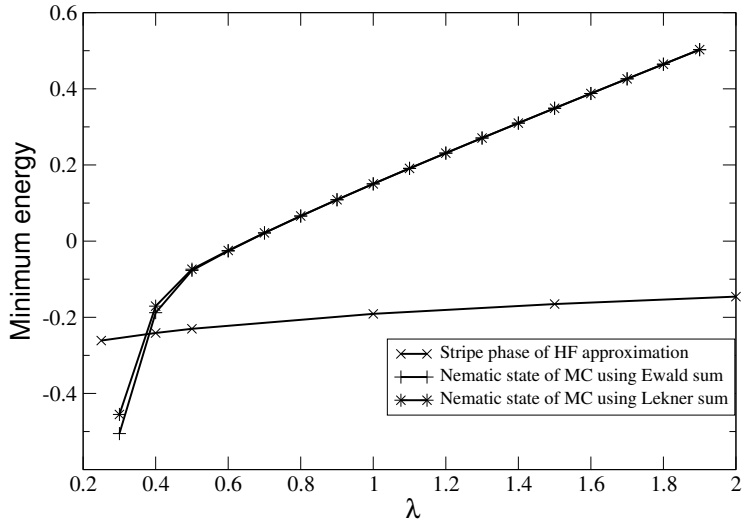

Figure 6.10: Comparison of the optimum nematic state obtained by using the pseudo-potential with Lekner and Ewald sum with the stripe state obtained from HF

As illustrated in Fig. 6.10, the values of critical λ obtained by Lekner and Ewald sum are quite close, and both are greater than 0.37. Thus one can conclude that with MC calculation, for $\lambda \leq \lambda_c = 0.37$, the energy of the nematic state is lower than the stripe-ordered state. The critical value of λ corresponding to the sample used in experiment [2] calculated in appendix B is approximately 0.34, which can be below the critical value found above. The critical value of λ_c we found from FHNC is 0.4 which is close to the one found from MC (see Fig. 6.11). Thus, both MC and FHNC calculations indicate that the nematic state might be the state observed experimentally for the 2DEG at the heterojunction in the samples used in

experiment [2].

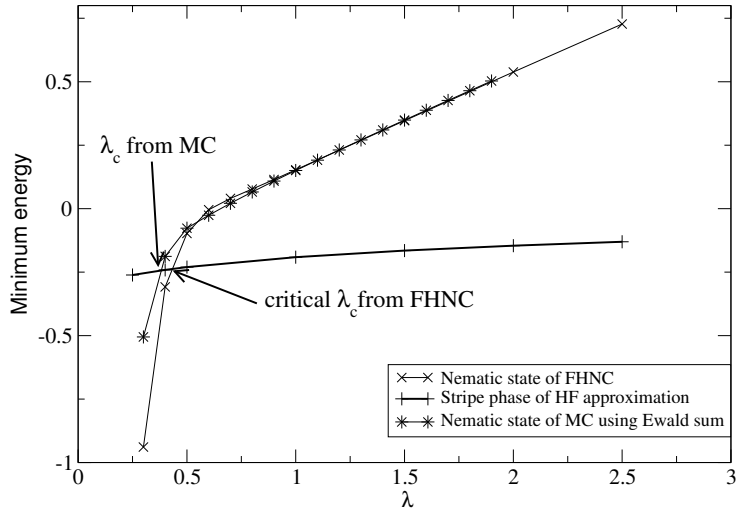

Figure 6.11: Comparison of the optimum nematic state obtained from FHNC and MC with the stripe state obtained from HF

There are two sources of error in our MC calculation. The first source of error is our assumption that the unprojected wavefunction is a good approximation of the original wavefunction in LLL, and, that is why we neglected the projection operator (equation 4.18). The second source of error is the finite size effects in our MC calculation. The values of energy we use in the comparison with the stripe-ordered phase and those of FHNC are obtained by running simulation on finite size systems of 121 up to 145 particles. The question one may ask is: does the difference in energy between the nematic state and the stripe state comes from the errors introduced by MC and HF?

We address this concern by comparing only the potential energies of the optimum nematic state with those of the stripe state and the isotropic state for the same values of λ (Fig. 6.12). We can see that the potential energies of the nematic state from MC calculation and the stripe phase from HF calculation are almost identical for $\lambda \geq 0.6$. Meanwhile, the difference between the results of MC for the isotropic state and those of HF for the stripe phase for

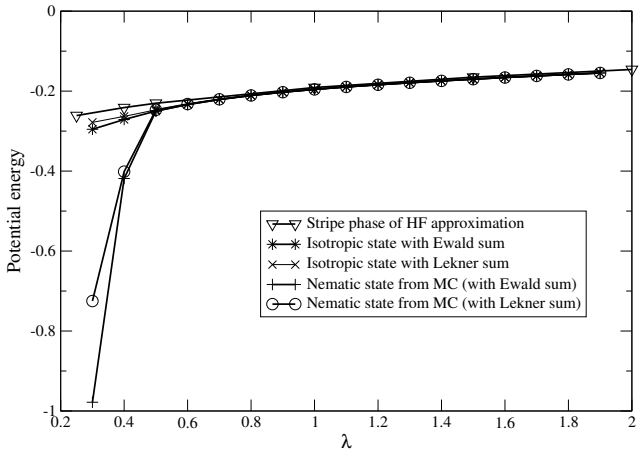

Figure 6.12: Comparison of the potential energies of optimum nematic state with the isotropic state and stripe state

all values of $\lambda \geq 0.3$ is quite small as compared to the difference between the nematic state of MC and stripe state of HF. Thus, one may argue that the difference between optimum energies of the nematic and stripe state within the range of $0.3 \leq \lambda \leq 0.6$ may not come from the difference between approximations of MC and HF, but, instead, it may come from the fact that at the 2^{nd} excited LL, the nematic state is energetically favorable.

CHAPTER 7

Hartree-Fock calculation of the stripe state

Another candidate for the anisotropy of the 2DEG is the stripe state. In order to find out what might be the true ground state that exhibits the anisotropic behavior of the 2DEG, we need to compare the energy of the stripe-ordered state with the one of the nematic state. Note that our calculations for the energy of the nematic state are done for a realistic potential which is more applicable for samples used in experiment in Ref. [2]. Thus, in this chapter, we want to compute the optimum energy of the stripe-ordered state using the same kind of potential. The stripe-ordered state is investigated extensively in [4], [5] and [49] using the Hartree-Fock approximation. However, the interaction potential used in these papers is a pure Coulomb interaction which does not take into account the finite confinement of the electron wavefunction along the z-direction. In this chapter, we will follow the same HF approximation using the Zhang-Das Sarma potential instead [16]. In the next section, we will discuss the stripe-ordered state. In section 7.2, we will discuss how to implement the HF, and in section 7.3, we will present the results. The results obtained in this chapter were used in comparison with those of the nematic state obtained from FHNC and MC (chapter 5 and 6).

7.1 The stripe-ordered state

It was shown in [4] and [5] that, at partially-filled high LL, a 2DEG under a high magnetic field can have a stripe or charge density wave (CDW) ground state in which the density of electron guiding centers has alternative uniform values. These values are piecewise constant along a periodic stripe structure. For example, for a system with filling factor of 9/2, these values are 4 and 5. Moreover, in [49], it was shown that the stripe state is indeed an

anisotropic triangular Wigner crystal (WC).

We will study WC lattices which can be parametrized as follows (see Fig. 7.1):

$$R_{nm} = na_1\hat{x} + (2m+n)a_2\hat{y}, \tag{7.1}$$

where

- n, m are integers,
- $a_1 = \sqrt{3}a/2\sqrt{1-\varepsilon}$ and $a_2 = \sqrt{1-\varepsilon}a/2$ are lattice constants,
- ε is the uniaxial anisotropic parameter of the lattice,
- $a = l_0(4\pi M/\sqrt{3}\nu)^{1/2}$ is the average lattice spacing (M is the number of electrons per bubble in a general bubble phase).

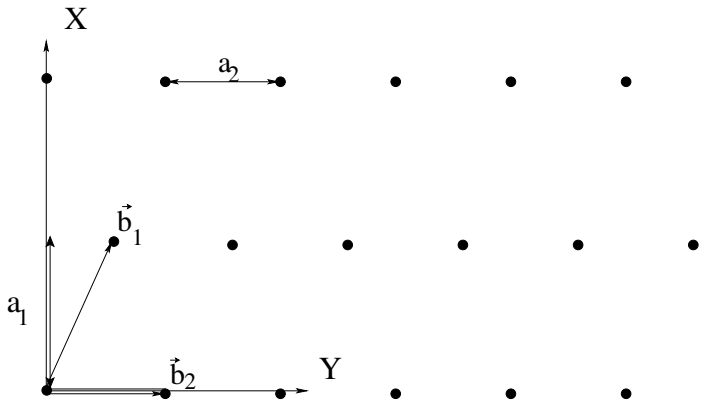

Figure 7.1: The anisotropic triangular WC lattice structure where $\vec{b}_1 = a_2\hat{x} + a_1\hat{y}$ and $\vec{b}_2 = a_1\hat{y}$

Fig. 7.2 taken from [49] illustrates WC lattices with various values of ε. Remember that $0 \leq \varepsilon \leq 1$, and $\varepsilon = 0$ corresponds to an isotropic triangular lattice.

7.2 Hartree-Fock approximation

In this section, we will briefly discuss the HF approximation to study the stripe-ordered state and present the formalism for a case of the Zhang-Das Sarma effective potential in which

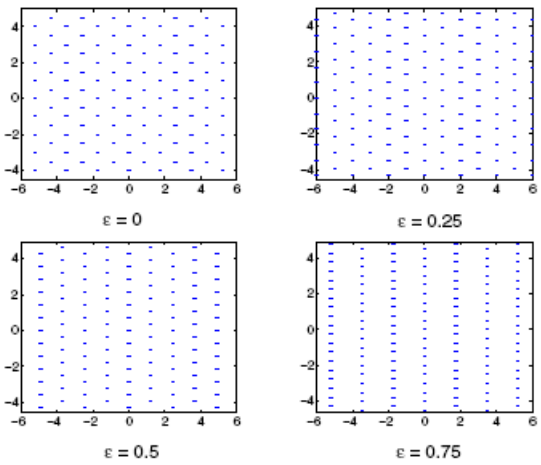

Figure 7.2: The anisotropic triangular WC lattice structure with various values of the uniaxial anisotropic parameter ε of the lattice defined in (7.1).

$\lambda > 0$. For a detailed development of this approach, one can refer to [5] and [4].

From [4], the self-consistent Hartree-Fock potential is given by:

$$U(\vec{q}) = \Big[H_{N,N}(\vec{q}) - X_{N,N}(\vec{q})\Big]\big\langle\rho(-\vec{q})\big\rangle \tag{7.2}$$

From [5], the Hartree and Fock terms are given as:

$$H(n_1, n_2, n_3, n_4, G) = \frac{1}{2\pi e^2 l_0} V(G) F_{n_1,n_2}(G) F_{n_3,n_4}(-G) \tag{7.3}$$

$$X(n_1, n_2, n_3, n_4, G) = \frac{1}{e^2 S} \sum_{\vec{q}} V(\vec{q}) F_{n_1,n_2}(\vec{q}) F_{n_3,n_4}(-\vec{q}) e^{-i\vec{q}\times G l_0^2}, \tag{7.4}$$

$$\tag{7.5}$$

where

$$F_{n\prime,n}(\vec{q}) = \left[\frac{n!}{n\prime!}\right]^{1/2} \left[\frac{(-q_y + iq_x)l_0}{\sqrt{2}}\right]^{n\prime-n} e^{-\frac{q^2 l_0^2}{4}} L_n^{n\prime-n}\left[\frac{q^2 l_0^2}{2}\right], \tag{7.6}$$

$$\vec{k}\times\vec{q} = k_x q_y - k_y q_x. \tag{7.7}$$

and n_1, n_2, n_3, n_4 are the LL. The potential $V(\vec{q})$ in our work is the Zhang-Das Sarma potential [16] and is given by:

$$V(\vec{q}) = \frac{e^2}{\epsilon l_0}\frac{2\pi}{q} e^{-\lambda q}. \tag{7.8}$$

In our case: $n_1 = n_2 = n_3 = n_4 = N$; then,

$$F_{N,N}(\vec{q}) = e^{-q^2 l_0^2/4} L_N\left(\frac{q^2 l_0^2}{2}\right) = F_{N,N}(-\vec{q}), \tag{7.9}$$

where $L_N(x)$ is the Laguerre polynomials of order N.

After some simple manipulations, one can derive:

$$H_{N,N}(\vec{G}) = \frac{e^2}{\epsilon l_0}\frac{e^{-\lambda G}}{G l_0} e^{-G^2 l_0^2/2}\left[L_N\left(\frac{G^2 l_0^2}{2}\right)\right]^2 \tag{7.10}$$

$$X_{N,N}(\vec{G}) = \frac{e^2}{\epsilon l_0}\int_0^\infty dx e^{-\lambda x/l_0} e^{-x^2/2}\left[L_N(x^2/2)\right]^2 J_0(xG). \tag{7.11}$$

where $J_0(x)$ is the zero-order Bessel function.

With those equations, we can carry out an iterative approach (which was described in detail in Refs. [4] and [5]) as follows:

1. Populate the reciprocal lattice vectors $\vec{G} = l_1\vec{k}_1 + l_2\vec{k}_2$ with

$$l_1 = -n_1, -(n_1 - 1), .., 0, .., n_1 \tag{7.12}$$

$$l_2 = -n_2, -(n_2 - 1), .., 0, .., n_2. \tag{7.13}$$

   where n_1, n_2 are integers.

2. Calculate $U(\vec{q})$ using (7.2). Initially, we set:

$$\left\langle \rho(\vec{q}) \right\rangle = \nu e^{-q^2 l_0^2/4}. \tag{7.14}$$

   This choice of initial values of $\left\langle \rho(\vec{q}) \right\rangle$ allows us to achieve self-consistence quickly.

3. Diagonalize the interaction matrix given by:

$$F_{\vec{G},\vec{G}'} \equiv U(\vec{G} - \vec{G}') e^{i\vec{G}\times\vec{G}' l_0^2/2}, \tag{7.15}$$

   to get the eigenvalues D and eigenvectors V. The single-particle Green's function is readily computed:

$$\left\langle \rho(\vec{G}) \right\rangle = \sum_j V_{G,j}[V^\dagger]_{j,\vec{G}=0}. \tag{7.16}$$

   The sum in the above equation is only carried out up to j that satisfies the following sum rule:

$$\left\langle \rho(\vec{G} = 0) \right\rangle = \nu \tag{7.17}$$

4. The new set values of $\langle\rho(\vec{G})\rangle$ will be used as the input values of (7.2).

This process is iterated until self-consistence $\langle\rho(\vec{G})\rangle$ is achieved. Finally, the interaction energy per particle is given as follows:

$$\frac{E_{HF}}{N_s} = \frac{1}{2\nu}\sum_{\vec{G}}\left[H_{N,N}(\vec{G})(1-\delta_{\vec{G},0}) - X_{N,N}(\vec{G})\right]|\langle\rho(\vec{G})\rangle|^2. \tag{7.18}$$

where N_s is the number of particles. Remember that, as usual we do not include the const value of $\hbar\omega_c/2$ in equation (7.18) since it is a common value for all states under our consideration.

7.3 Results and Discussion

In our work, we populate reciprocal lattice vectors using $n_1 = 25$ and $n_2 = 15$. With these populated reciprocal lattices, we can satisfy the sum rule (7.17) to more than 8 digit after the point. Self-consistent of the HF is usually achieved after 20 iterations.

As a test of our HF implementation, we want to investigate the phase diagram of the bubble phase for filling factor $0.15 \leq \nu \leq 0.5$ at the 2^{nd} excited LL and compare it with the one found in Ref. [49]. We calculate the energy at different filling factors ($0.15 \leq \nu \leq 0.5$) and for different bubble phases ($M = 1, 2, 3$). For a fixed filling factor ν and a bubble phase M, we find the optimum energy with respect to ε. Note that, the potential energy we are trying to minimize with respect to ε is the pure Coulomb potential ($\lambda = 0$).

First, for the bubble phase ($M > 1$), we find that the optimum energy always corresponds to the case of $\varepsilon = 0$. Second, we found that at half-filled LL the WC ($M = 1$) is more stable than other bubble phases ($M > 1$). In Fig. 7.3, we compare the optimum energy of the stripe-ordered and bubble states as function of ν with the ones obtained by Ettouhami et al. in Ref. [49]. As it can be seen, our phase diagram is in exact agreement with [49].

The anisotropy parameter ε, which minimizes the energy of the WC state in equation (7.18), is plotted in Fig. 7.4 as a function of ν. We found that, at half-filling, with $\varepsilon = 0.7$, the energy of the stripe state is minimum. In addition, we also found that, this value $\varepsilon = 0.7$ is

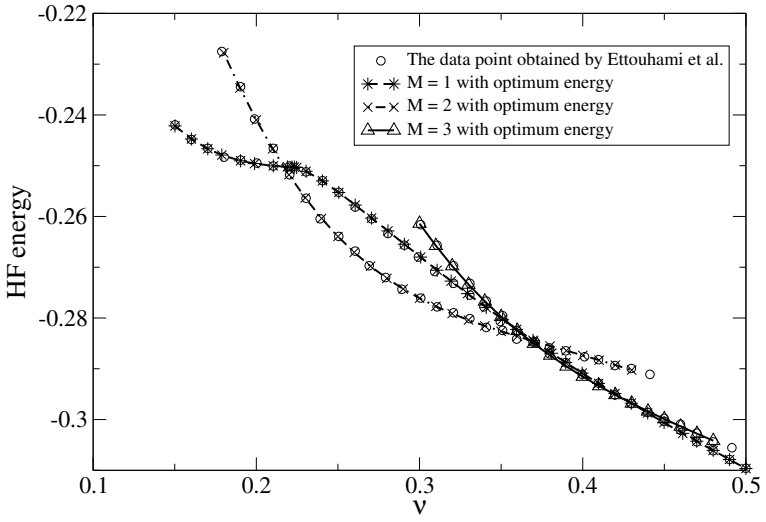

Figure 7.3: Optimum energies of WC, 2e bubble solid, and 3e buble solid at the 2^{nd} excited LL as a function of ν

also the optimum value at other values of $\lambda > 0$. Thus, all values of the optimum energy of the stripe state at various values of λ are calculated using $\varepsilon = 0.7$. Obtained values of the optimum stripe state energy are reproted in table 7.1.

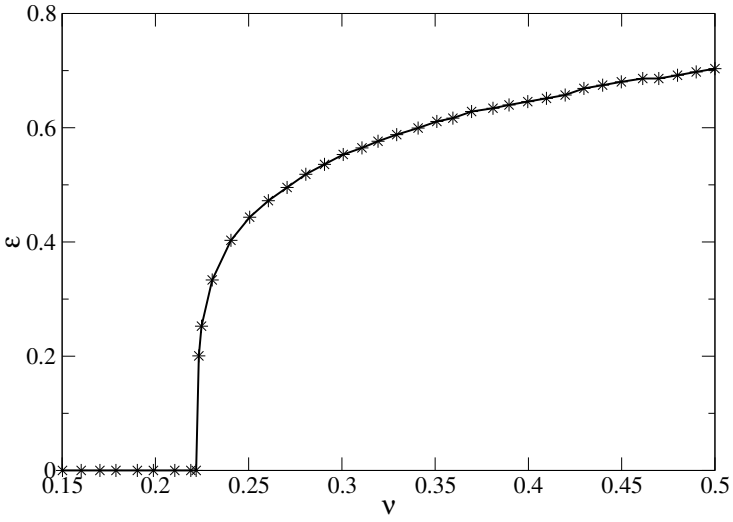

Figure 7.4: Values of the anisotropy parameter ε that minimize the energy of the WC as a function of ν

Table 7.1: Optimum values of the energy of the stripe state as a function of λ at the second excited LL obtained from HF calculation.

λ (in unit of l_0)	Potential energy (in unit of $e^2/\epsilon_0 l_0$)
0.25	-0.2611518474
0.40	-0.2412068895
0.50	-0.2302259171
1.00	-0.1910215546
1.50	-0.1651717639
2.00	-0.1457949674
2.50	-0.1303652027

CHAPTER 8

Summary and Outlook

We have used variational methods to study the instability of the nematic state as the ground state of the two dimensional-electron gas (2DEG) at a filling factor of 1/2 and up to the 2^{nd} excited LL. An anisotropic behavior in the transport of the 2DEG at half-filling fraction and at low temperature was discovered by Lilly et al. [2] and Du et al. [3]. Since then this discovery has been a subject of numerous theoretical works. Fradkin, Kivelson, Manousakis and Nho in [7] studied the nematic phase with a symmetry breaking field using a classical MC simulation. Their success strongly motivated us to study the nematic state as a possible ground state of the 2DEG. Our work uses the proposed ground state wavefunction of the nematic state by Oganesyan et al. [15] as the ansatz wavefunction. This wavefunction is based on the ground state wavefunction of the 2DEG at half-filling proposed by Rezayi and Read [12]. The symmetry breaking parameter is the ratio of wave vectors characterizing the deformation of the Fermi sea, $\alpha = k_1/k_2$, where k_1, k_2 are the semimajor and semiminor axes of the elliptical Fermi sea (the Fermi surface of the nematic phase is an ellipse as opposed to a circle in the isotropic phase). We use this trial wavefunction to study the instability of the nematic state up to the 2^{nd} excited LL with α as the variational parameter. In our work, we study the unprojected version of the wavefunction, thus making the assumption that it is a good approximation of the original wavefunction.

The stripe-ordered state can also be considered to possibly account for the anisotropy of the 2DEG at the second excited LL. So far this state has been intensively studied using the HF approximation. It is very important in our work to compare the nematic state's energies with the stripe-ordered state to draw a conclusion about the stability of the nematic state of the 2DEG. In this thesis, we carried out the HF for this state using what we refer to as the Zhang-Das Sarma potential [16], which is more realistic since it takes into account the

finite confinement of the wavefunction along the z-direction characterized by the parameter λ.

To calculate the potential energy of the nematic state we used two variational approaches. The first one is FHNC/0 which has been applied successfully to study other quantum fluid systems. This method is applied for infinite systems, however this method can be a good approximation only for low density systems. With this limitation in mind it is very important to compare the results of this method with other reliable methods. The second method we used is MC. While with MC, one is not subjected to the low density limit which restricts the FHNC/0, it can only be done for a finite-size system. In our work it is not trivial to extrapolate from the results of a finite-size system to the thermodynamic limit. However, the calculations presented here indicate that, the results obtained for a system of more than 100 particles do not change noticeably with the size of the system. We will compare the results and the conclusions obtained from both methods.

With FHNC/0, we computed the pair distribution function for the LLL and used the single-LL approximation to calculate the potential energy at high LLs using an effective Zhang-Das Sarma potential. Our results indicated that for the LLL and the first excited LL, the isotropic state is always energetically favorable relative to the nematic state. For the second excited LL, we found that for a range values of $\lambda \leq 0.6$, the nematic phase is energetically favorable as compared to the isotropic state. Next, we compared the optimal energy of the nematic phase with that of the stripe state at various value of λ and found that the nematic state is more stable at $\lambda \leq 0.4$. It is interesting to estimate the value of λ which corresponds to the samples used in the experiments to examine if it falls inside or outside this interval. Following the calculation presented in [16] using the values of electron density for the samples used in [2] we found that $\lambda \sim 62\mathring{A}$ which is about 0.34 in units of the magnetic length l_0. Thus, within our FHNC/0 results we concluded that the quantum nematic state might be energetically lower than the stripe ordered or bubble phases for the 2DEG in the sample used in [2].

With MC, we used a square geometry instead of a disk geometry. We chose the square geometry because it is more natural to use for the case of the ground state wavefunction of the nematic phase. As a test of our method, we used this geometry to study the FQHE system with a filling factor of 1/3; the results we obtained are exactly the same as the ones obtained by Morf and Halperin [1] using the disk geometry. We computed the pair

distribution function, the potential energy and the total energy of the nematic phase with various values of anisotropic parameters α and "thickness" parameter λ. We found that the isotropic state is always energetically more stable than the nematic state at LLL and the first excited LL. At the second excited LL, the nematic state is energetically lower than the isotropic state for $\lambda \leq \lambda_c \simeq 0.4$. Finally, we compared the optimum energy of the nematic state obtained by MC with that of the stripe ordered state and found that the optimum energy of the nematic state is below that of the stripe state for $\lambda \leq \lambda_c \simeq 0.37$. Therefore, since the value of λ which corresponds to the experimental case of Ref. [2] is 0.34, we concluded, that the nematic state is energetically favorable as compared to the stripe-ordered state for the 2DEG in the heterojunction used in [2]. In addition, it is interesting to probe this transition from the nematic to stripe to isotropic state either by experimentally altering the value of λ or by means of an in-plane magnetic field.

Because the HF predicts a stripe state, the observed anisotropy of the transport properties of the 2DEG were considered as a signature of the stripe-ordered state. This state breaks both translational invariance in one direction and rotational invariance. The finite size diagonalizations of Haldane, Rezayi and Yang [60] are also usually interpreted as a stripe state. However, the systems they can do are very small, and, in addition toroidal boundary conditions were used which also break rotational invariance. Thus it implies that with these limitations they cannot conclusively say if the true ground state is stripe or nematic. In our calculation we find that the optimum nematic phase corresponds to an anisotropy parameter $\alpha \sim 10$ near the physically realized value of parameter λ. That means that with such large anisotropy it is impossible to distinguish the nematic state from the stripe state in systems with only as small number of electrons which are only accessible by finite-size diagonalization [60].

APPENDIX A

Evaluation of kinetic energy of the nematic state

In this appendix, we want to show the formalism of the kinetic energy difference between the nematic and the isotropic state. In the single-LL approximation, the kinetic energy is quenched. In addition, the same is true in the HF treatment of the stripe, namely, there is no kinetic energy due to any correlation factors or operators. While this approximation gives a significant difference between the potential energy of the isotropic state and the nematic state, it gives no difference between their kinetic energy which is unacceptable because of the difference in the geometry of the Fermi sea. We want to estimate this differece. We can start with:

$$(\vec{\nabla} - \vec{A})^2 F\Phi \tag{A.1}$$

$$= (\vec{\nabla} - \vec{A})^2 F\Phi + 2\Big[(\vec{\nabla} - \vec{A})F\Big]\nabla\Phi + F\nabla^2\Phi \tag{A.2}$$

The first term in the above equation yields:

$$(\vec{\nabla} - \vec{A})^2 F\Phi = \frac{\hbar\omega_c}{2} F\Phi, \tag{A.3}$$

which is common for all states under our consideration so for simplicity we can drop it. The last term is:

$$F\nabla^2\Phi = F\sum_k \frac{\hbar^2 k^2}{2m^\star}\Phi \tag{A.4}$$

So the contribution of the last term is:

$$\sum_k \frac{\hbar^2 k^2}{2m^\star} \tag{A.5}$$

Then the difference between kinetic energy of the anisotropic and the isotropic state comes from this term, namely:

$$\Delta_{KE} = \frac{1}{N}\left(\sum_{isotropic\,\vec{k}} \frac{\hbar^2 k^2}{2m^\star} - \sum_{anisotropic\,\vec{k}} \frac{\hbar^2 k^2}{2m^\star} \right) \tag{A.6}$$

First, considet the isotropic term:

$$\frac{1}{N}\sum_{k} \frac{\hbar^2 k^2}{2m^\star} \tag{A.7}$$

For infinite systems, we sum all over states inside the Fermi circular surface

$$\sum_{\vec{k}} k^2 \to \frac{A}{(2\pi)^2}\int k^2 d^2k \tag{A.8}$$

Thus:

$$\frac{1}{N}\sum_{\vec{k}} \frac{\hbar^2 k^2}{2m^\star} = \frac{\hbar^4 k_F^4}{16 m^\star \pi \rho} \tag{A.9}$$

Using $k_F^2 = 4\pi\rho$, one can obtain the kinetic energy of the isotropic state:

$$\frac{1}{N}\sum_{k} \frac{\hbar^2 k^2}{2m^\star} = \frac{\hbar^2 k_F^2}{4m^\star} \tag{A.10}$$

For the anisotropic term:

$$\frac{1}{N}\sum_{\vec{k}} \frac{\hbar^2 k^2}{2m^\star}, \tag{A.11}$$

we carry the sum over all states inside the elliptical Fermi sea and obtain:

$$\frac{1}{N}\sum_{\vec{k}} \frac{\hbar^2 k^2}{2m^\star} = \frac{\hbar^2 k_F^2}{\rho 16 m^\star \pi}\left(\frac{k_1^2 + k_2^2}{2}\right) \tag{A.12}$$

Using $k_F^2 = 4\pi\rho$, the anisotropic term now is:

$$\frac{1}{N}\sum_{\vec{k}} \frac{\hbar^2 k^2}{2m^\star} = \frac{\hbar^2}{4m^\star}\frac{k_1^2 + k_2^2}{2} \tag{A.13}$$

Using the facts that $k_F^2 = k_1 \cdot k_2$ and $k_1/k_2 = \alpha$, the kinetic energy difference between the isotropic state and the nematic state is given as follows:

$$\Delta_K = -\frac{\hbar^2 k_F^2}{4m^\star}\frac{(1-\alpha)^2}{2\alpha} \tag{A.14}$$

APPENDIX B

Characteristic Scale Values

In this appendix, we will present the numerical values of some important quantities which are often used in our calculations and comparisons with the experiments and show how they rescale with respect to the experimental quantities such as the magnetic field $\vec{B}$. We also show the estimation of the value of λ for the materials used in the experiment [2]. This calculation is outlined in Ref. [16].

- The values of Coulomb energy is reported in terms of:

$$\frac{e^2}{\epsilon l_0} = 51.67K^0\sqrt{B[T]}, \tag{B.1}$$

  where ϵ is the dielectric constant and for the case of GaAs $\epsilon = 12.6$. And $l_0 = \sqrt{\hbar c/eB}$ is the magnetic length.

- Cyclotron energy is:

$$\hbar\omega_c = \frac{\hbar eB}{m^\star c}, \tag{B.2}$$

$$\tag{B.3}$$

  or,

$$\hbar\omega_c[meV] = 1.728B[T], \tag{B.4}$$

  where $m^\star = 0.067m_e$ is the effective mass of the electron.

- The kinetic energy difference Δ_K is expressed in units of $\hbar^2k_F^2/4m^\star$ where, for our system $k_F = 1/l_0$, thus, one can obtain:

$$\left[\Delta_K\right] = \frac{\hbar^2}{4m^\star l_0^2} = \frac{\hbar eB}{4m^\star c} \tag{B.5}$$

$$= \frac{1.728}{4}meV = 4.32K^0 = 0.0836\left[\frac{e^2}{\epsilon l_0}\right]\sqrt{B[T]} \tag{B.6}$$

- A value of λ can be estimated for the experimental samples used in paper by Du and Lilly [2] by following the steps in [16]. Specifically:

$$\lambda = 1.5 \cdot b^{-1} \tag{B.7}$$

where

$$b^{-1} = 40.2 \cdot N^{\star -1/3}, \tag{B.8}$$

$$N^{\star} = N_d + \frac{11}{32} N_s. \tag{B.9}$$

For the samples used in the experiment in Ref. [2]:

$$N_d = 0, \tag{B.10}$$

$$N_s = 2.67(10^{11} cm^{-2}). \tag{B.11}$$

Thus,

$$\lambda_0 = 62 \mathring{A} \tag{B.12}$$

- Remember that in our calculations, λ and other length quantities (e.g. x,y..) are evaluated in units of l_0.

- $l_0 = (\frac{\hbar c}{eB})^{1/2}$. For $B = 1T$, $l_0 = 256.6 \mathring{A}$, for the case of the experiments [2] with $B = 2T$, $l_0 \sim 181 \mathring{A}$. That means that, in the units of l_0 the values of λ at which the nematic state is observed in the experiment is $\lambda \approx 0.34$ for a magnetic field of $2T$

APPENDIX C

Technical issues of implementation of FHNC

In this appendix, we discuss certain technical details applied in the FHNC iteration procedure. We find that for higher LL, we needed to solve the FHNC equations using a combination of real and momentum spaces and, in addition, a multigrid method because of the combination of the short-range large-amplitude oscillations (and, as a consequence, large cancellations) and the long-range small-amplitude oscillations.

We are interested in the energy difference between the isotropic and the anisotropic state as a function of λ and α for L=0, L=1, L=2. In the interesting region, the energy differences between the nematic and the isotropic state is indeed very small relative to the energy e^2/l_0, so very high accuracy is required in the present calculation. The effective potential (5.2) for high LL and for small values of λ changes rapidly at small distances and oscillates slowly at large distances (see Figs. C.1 and C.3). In Figs. C.1,C.3, the quantity $F(r) = [g(r)1]V_{eff}^{L=2}(r)$ which is integrated in Eq. (5.1) is shown and the integrand $rF(r)$ is also presented in Figs. C.2,C.4 in order to illustrate this feature. Notice that in order to capture the short-range oscillations a very fine mesh is required, and we need to integrate up to large distances in order to capture the long-distance fluctuations. In addition, because this oscillatory behavior causes large cancellations in calculating the potential energy using Eq. (5.1), the energy is a small number relative to the contribution of each of the oscillations. Therefore, the small-amplitude much slower oscillations at long distances have non-negligible contribution to the small energy difference given by Eq. (5.33). Because these are slow and of much smaller amplitude oscillations, the long-distance contribution can be included with a wider size mesh as compared to the grid size required for short-range oscillations. Hence, it is important to use a small enough size mesh at small distances and to include large enough distances with a much wider mesh. The FHNC equations were solved using an adaptive mesh to incorporate

these multiscale oscillations accurately (see Figs. C.2,C.4, and the discussions in the figure captions). In order to keep ourselves within realistic computational time scales, we needed to limit the range of our mesh size and, thus, our results can only be trusted for values of $\lambda \geq 0.25$.

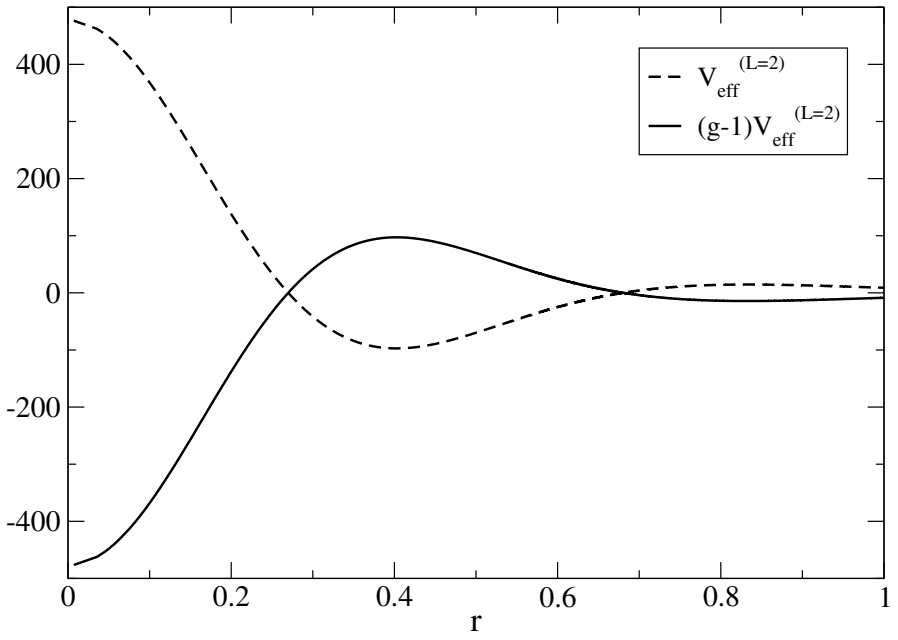

Figure C.1: The effective potential $V_{eff}^{(L=2)}(r)$ and $(g-1)V_{eff}^{(L=2)}(r)$ for $0 < r < 1$

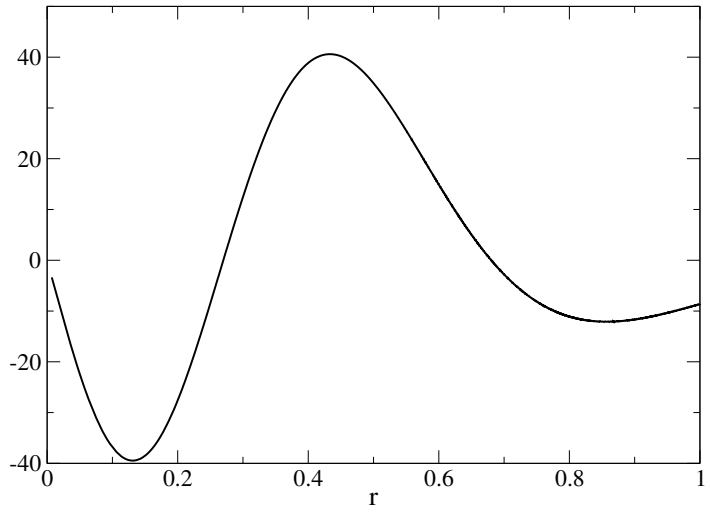

Figure C.2: The integrand $r(g-1)V_{eff}^{(L=2)}(r)$ used to calculate the potential energy is shown for $0 < r < 1$. Notice that there are large scale cancellations due to its rapid fluctuation at small values of r

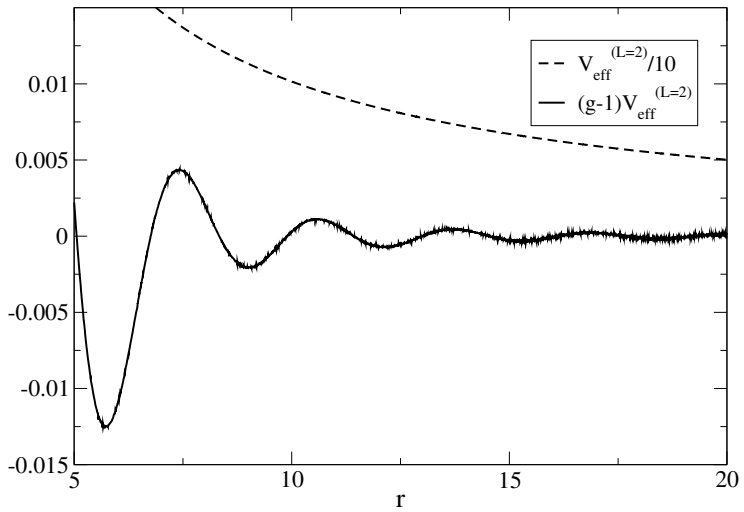

Figure C.3: The effective potential $V_{eff}^{(L=2)}(r)$ and $(g-1)V_{eff}^{(L=2)}(r)$ for $5 < r < 20$

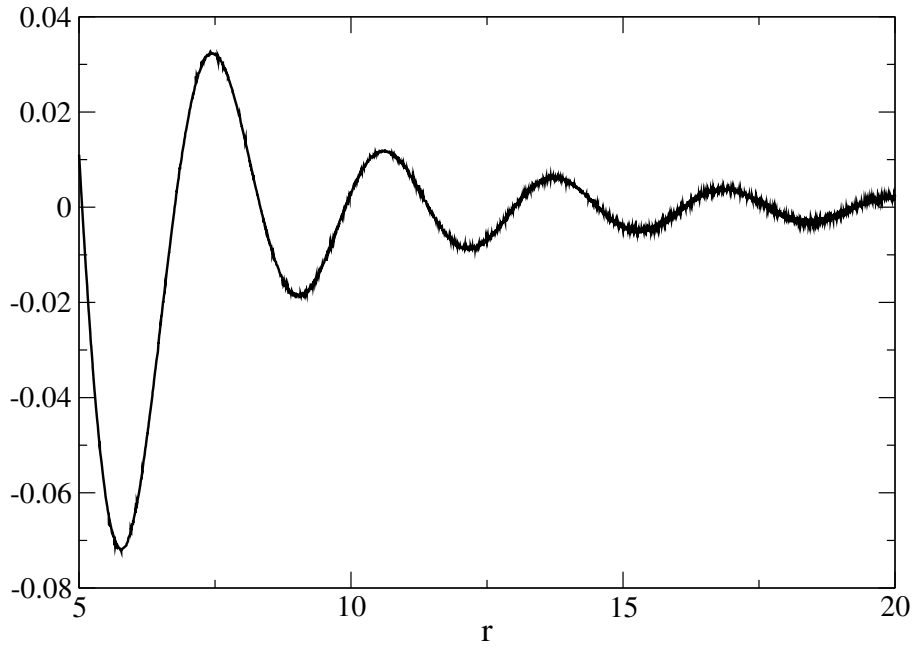

Figure C.4: The integrand $r(g-1)V_{eff}^{(L=2)}(r)$ used to calculate the potential energy is shown for $5 < r < 20$. Notice that there are cancellations due to long range fluctuation due to $g-1$ at large distance

APPENDIX D

Tables of values of energies obtained from FHNC/O calculation

This appendix contains all the tables of values of potential energies and total energies obtained from FHNC/0 calculation.

Table D.1: Potential energy values of nematic states with various values of λ and $1 \leq \alpha \leq 5$. Note that $\alpha = 1$ is the isotropic phase at the LLL.

λ	$\alpha = 1$	$\alpha = 2$	$\alpha = 3$	$\alpha = 4$	$\alpha = 5$
0.1	-0.487207	-0.479849	-0.473117	-0.469272	-0.467323
0.3	-0.453017	-0.445731	-0.439098	-0.435321	-0.433415
0.3	-0.442238	-0.43499	-0.428407	-0.424666	-0.422781
0.4	-0.421578	-0.41443	-0.407975	-0.40432	-0.402487
0.5	-0.402082	-0.395065	-0.388768	-0.385217	-0.383447
0.6	-0.383705	-0.376847	-0.370734	-0.367302	-0.365602
0.7	-0.366396	-0.359722	-0.353815	-0.350512	-0.348888
0.8	-0.350104	-0.343636	-0.337952	-0.334786	-0.333239
0.9	-0.334774	-0.328531	-0.323082	-0.320057	-0.31859
1	-0.320354	-0.31435	-0.309145	-0.306262	-0.304876
1.5	-0.260133	-0.255406	-0.251424	-0.249223	-0.248208
2	-0.21559	-0.212048	-0.209127	-0.207482	-0.206761
2.5	-0.18222	-0.179627	-0.177526	-0.176297	-0.175792

We report the values of the potential energy and total energy at the second excited LL, remember that our values can be trusted only for $\lambda \geq 0.3$.

Table D.2: Potential energy values of nematic states with various values of λ and $6 \leq \alpha \leq 9$ at the LLL.

λ	$\alpha = 6$	$\alpha = 7$	$\alpha = 8$	$\alpha = 9$
0.1	-0.465744	-0.464318	-0.463806	-0.462926
0.3	-0.431873	-0.43048	-0.429981	-0.429125
0.3	-0.421257	-0.419882	-0.419389	-0.418544
0.4	-0.401007	-0.399672	-0.399193	-0.398376
0.5	-0.382018	-0.38073	-0.380268	-0.379483
0.6	-0.36423	-0.362993	-0.36255	-0.361799
0.7	-0.347576	-0.346395	-0.345971	-0.345257
0.8	-0.331991	-0.330865	-0.330461	-0.329784
0.9	-0.317405	-0.316336	-0.315952	-0.315312
1	-0.303754	-0.302739	-0.302376	-0.301771
1.5	-0.247374	-0.246607	-0.246334	-0.245889
2	-0.206148	-0.20557	-0.205366	-0.205041
2.5	-0.17534	-0.174898	-0.174745	-0.174506

Table D.3: Potential energy values of nematic states with various values of λ and $1 \leq \alpha \leq 5$ at the first excited LL. Note that $\alpha = 1$ is the isotropic phase.

λ	$\alpha = 1$	$\alpha = 2$	$\alpha = 3$	$\alpha = 4$	$\alpha = 5$
0.1	-0.325699	-0.316824	-0.303747	-0.293834	-0.287627
0.3	-0.307843	-0.294177	-0.280492	-0.272315	-0.267845
0.3	-0.302247	-0.288257	-0.275127	-0.26772	-0.263855
0.4	-0.291543	-0.277883	-0.266267	-0.260328	-0.257509
0.5	-0.281408	-0.26881	-0.258845	-0.254145	-0.252113
0.6	-0.27179	-0.260546	-0.252122	-0.248392	-0.246913
0.7	-0.262657	-0.252807	-0.245721	-0.242717	-0.241609
0.8	-0.253979	-0.245436	-0.239463	-0.236991	-0.236123
0.9	-0.245726	-0.238347	-0.233279	-0.231189	-0.230473
1	-0.237868	-0.231495	-0.227155	-0.22534	-0.224718
1.5	-0.203706	-0.200409	-0.198043	-0.196838	-0.196381
2	-0.176518	-0.174486	-0.172906	-0.171951	-0.171585
2.5	-0.154701	-0.153276	-0.152137	-0.151372	-0.1511

Table D.4: Potential energy values of nematic states with various values of λ and $6 \leq \alpha \leq 9$ at the first excited LL.

λ	$\alpha = 6$	$\alpha = 7$	$\alpha = 8$	$\alpha = 9$
0.1	-0.282178	-0.276807	-0.274907	-0.271107
0.3	-0.264283	-0.261306	-0.260062	-0.25826
0.3	-0.260871	-0.258486	-0.257479	-0.256125
0.4	-0.255463	-0.25395	-0.253322	-0.25258
0.5	-0.250719	-0.249745	-0.249359	-0.248954
0.6	-0.24594	-0.245276	-0.245029	-0.244788
0.7	-0.240893	-0.240394	-0.240217	-0.240044
0.8	-0.235556	-0.235134	-0.234988	-0.234833
0.9	-0.229987	-0.229596	-0.229461	-0.2293
1	-0.224274	-0.22389	-0.223755	-0.22358
1.5	-0.195983	-0.195586	-0.195444	-0.195233
2	-0.171238	-0.170883	-0.170759	-0.170573
2.5	-0.150819	-0.150521	-0.150421	-0.150271

Table D.5: Potential energy values of nematic state with various values of λ and $1 \leq \alpha \leq 5$ at the second excited LL. Note that $\alpha = 1$ is the isotropic phase.

λ	$\alpha = 1$	$\alpha = 2$	$\alpha = 3$	$\alpha = 4$	$\alpha = 5$
0.1	0.548765	-0.683934	-1.76367	-2.5492	-3.21978
0.3	-0.100093	-0.437593	-0.764279	-1.02915	-1.24331
0.3	-0.213081	-0.415728	-0.663619	-0.855875	-1.0037
0.4	-0.248757	-0.353171	-0.499354	-0.59993	-0.668064
0.5	-0.217748	-0.298189	-0.384723	-0.436043	-0.465196
0.6	-0.204315	-0.263152	-0.314179	-0.339323	-0.350075
0.7	-0.201274	-0.240746	-0.27067	-0.282156	-0.284687
0.8	-0.199432	-0.225058	-0.242469	-0.247	-0.246195
0.9	-0.196639	-0.213241	-0.22324	-0.224354	-0.222458
1	-0.193039	-0.203876	-0.209485	-0.209017	-0.206992
1.5	-0.172418	-0.173626	-0.173341	-0.172223	-0.171508
2	-0.153659	-0.153364	-0.152724	-0.152016	-0.151743
2.5	-0.137659	-0.137082	-0.136516	-0.13598	-0.135823

Table D.6: Potential energy values of nematic state with various values of λ and $6 \leq \alpha \leq 9$ at the second excited LL.

λ	$\alpha = 6$	$\alpha = 7$	$\alpha = 8$	$\alpha = 9$
0.1	-3.91382	-4.42977	-5.17749	-5.6919
0.3	-1.44892	-1.59407	-1.76645	-1.87751
0.3	-1.13907	-1.22668	-1.33133	-1.38895
0.4	-0.723015	-0.748836	-0.783449	-0.790272
0.5	-0.484096	-0.486103	-0.493974	-0.485905
0.6	-0.353866	-0.348357	-0.34723	-0.337235
0.7	-0.282876	-0.276219	-0.272933	-0.264819
0.8	-0.242857	-0.237162	-0.234047	-0.228335
0.9	-0.219179	-0.214868	-0.212508	-0.208752
1	-0.204272	-0.201186	-0.199561	-0.197175
1.5	-0.170841	-0.170251	-0.170047	-0.169754
2	-0.151464	-0.151178	-0.151092	-0.150959
2.5	-0.135625	-0.135398	-0.135328	-0.135224

Table D.7: Total energy values of nematic states with various values of λ and $1 \leq \alpha \leq 5$ at the second excited LL. Note that $\alpha = 1$ is the isotropic phase.

λ	$\alpha = 1$	$\alpha = 2$	$\alpha = 3$	$\alpha = 4$	$\alpha = 5$
0.1	0.583365	-0.640684	-1.70601	-2.47568	-3.12982
0.3	-0.013594	-0.329469	-0.620114	-0.845337	-1.01841
0.3	-0.109282	-0.285979	-0.490621	-0.635302	-0.733819
0.4	-0.110359	-0.180173	-0.26869	-0.305833	-0.308228
0.5	-0.04475	-0.081942	-0.096393	-0.068423	-0.015401
0.6	0.003283	-0.003655	0.031817	0.101822	0.189679
0.7	0.040924	0.062001	0.132992	0.232513	0.345026
0.8	0.077365	0.120938	0.218859	0.341193	0.473477
0.9	0.114757	0.176004	0.295754	0.437363	0.587173
1	0.152958	0.228619	0.367176	0.526225	0.692598
1.5	0.346576	0.475117	0.691649	0.93064	1.17788
2	0.538333	0.711626	1.0006	1.31847	1.64744
2.5	0.727331	0.944156	1.30513	1.70212	2.11315

Table D.8: Total energy values of nematic states with various values of λ and $5 \leq \alpha \leq 10$ at the second excited LL. Note that $\alpha = 1$ is the isotropic phase.

λ	$\alpha = 1$	$\alpha = 2$	$\alpha = 3$	$\alpha = 4$	$\alpha = 5$
0.1	0.583365	-0.640684	-1.70601	-2.47568	-3.12982
0.3	-0.013594	-0.329469	-0.620114	-0.845337	-1.01841
0.3	-0.109282	-0.285979	-0.490621	-0.635302	-0.733819
0.4	-0.110359	-0.180173	-0.26869	-0.305833	-0.308228
0.5	-0.04475	-0.081942	-0.096393	-0.068423	-0.015401
0.6	0.003283	-0.003655	0.031817	0.101822	0.189679
0.7	0.040924	0.062001	0.132992	0.232513	0.345026
0.8	0.077365	0.120938	0.218859	0.341193	0.473477
0.9	0.114757	0.176004	0.295754	0.437363	0.587173
1	0.152958	0.228619	0.367176	0.526225	0.692598
1.5	0.346576	0.475117	0.691649	0.93064	1.17788
2	0.538333	0.711626	1.0006	1.31847	1.64744
2.5	0.727331	0.944156	1.30513	1.70212	2.11315

APPENDIX E

Tables of values of energies obtained from MC calculation

This appendix contains all the tables of values of potential energies and total energies obtained from MC calculation. The values reported are obtained from MC simulation using the Ewald summation technique. As pointed out in the chapter 6 the Ewald summation technique also yields the same pseudo-potential as the Lekner summation technique.

We report the values of the potential energy and the total energy at the second excited LL.

Table E.1: Potential energy values of nematic state with various values of λ and $1 \leq \alpha \leq 5$ at the LLL. Note that $\alpha = 1$ is the isotropic phase.

λ	$\alpha = 1$	$\alpha = 2$	$\alpha = 3$	$\alpha = 4$	$\alpha = 5$
0.3	-0.432917	-0.429721	-0.424163	-0.423668	-0.422633
0.4	-0.412321	-0.409214	-0.403818	-0.403337	-0.402336
0.5	-0.392913	-0.389915	-0.384712	-0.384248	-0.383287
0.6	-0.374649	-0.371774	-0.36679	-0.366345	-0.365429
0.7	-0.357476	-0.354737	-0.349991	-0.349566	-0.348697
0.8	-0.341343	-0.338747	-0.33425	-0.333846	-0.333027
0.9	-0.326195	-0.323746	-0.319505	-0.319122	-0.318352
1	-0.311975	-0.309675	-0.305693	-0.30533	-0.304609
1.1	-0.298629	-0.296478	-0.292751	-0.292409	-0.291736
1.2	-0.286103	-0.284099	-0.280622	-0.280299	-0.279672
1.3	-0.274345	-0.272483	-0.26925	-0.268945	-0.268362
1.4	-0.263306	-0.261581	-0.25858	-0.258294	-0.257752
1.5	-0.252937	-0.251343	-0.248565	-0.248295	-0.247792
1.6	-0.243193	-0.241723	-0.239156	-0.238902	-0.238437
1.7	-0.234032	-0.23268	-0.230311	-0.230073	-0.229641
1.8	-0.225414	-0.224172	-0.22199	-0.221765	-0.221366
1.9	-0.217302	-0.216162	-0.214154	-0.213943	-0.213574
2	-0.209659	-0.208616	-0.206769	-0.206571	-0.20623
2.1	-0.202455	-0.2015	-0.199804	-0.199618	-0.199302
2.2	-0.195658	-0.194785	-0.193228	-0.193053	-0.192761
2.3	-0.18924	-0.188443	-0.187015	-0.18685	-0.18658
2.4	-0.183175	-0.182448	-0.181138	-0.180984	-0.180734

Table E.2: Potential energy values of nematic state with various values of λ and $6 \leq \alpha \leq 9$ at the LLL.

λ	$\alpha = 6$	$\alpha = 7$	$\alpha = 8$	$\alpha = 9$
0.4	-0.402329	-0.402311	-0.401879	-0.400947
0.5	-0.383283	-0.38326	-0.382845	-0.381949
0.6	-0.365426	-0.365399	-0.365003	-0.364147
0.7	-0.348695	-0.348663	-0.348287	-0.347474
0.8	-0.333024	-0.332989	-0.332634	-0.331865
0.9	-0.31835	-0.318311	-0.317976	-0.317252
1	-0.304607	-0.304565	-0.30425	-0.30357

Table E.3: Potential energy values of nematic state with various values of λ and $1 \leq \alpha \leq 5$ at the first exited LL. Note that $\alpha = 1$ is the isotropic phase.

λ	$\alpha = 1$	$\alpha = 2$	$\alpha = 3$	$\alpha = 4$	$\alpha = 5$
0.3	-0.288148	-0.28132	-0.269529	-0.268581	-0.266193
0.4	-0.276789	-0.271289	-0.262108	-0.261468	-0.259865
0.5	-0.266846	-0.262499	-0.255478	-0.255053	-0.254034
0.6	-0.257888	-0.254498	-0.249183	-0.248897	-0.248275
0.7	-0.249637	-0.247017	-0.243008	-0.242805	-0.242434
0.8	-0.241913	-0.239901	-0.23687	-0.236714	-0.236489
0.9	-0.234604	-0.233063	-0.230752	-0.230619	-0.230473
1	-0.227638	-0.226457	-0.224672	-0.224548	-0.224436
1.1	-0.220971	-0.220063	-0.218657	-0.218533	-0.218433
1.2	-0.214574	-0.213869	-0.212736	-0.212611	-0.212508
1.3	-0.208428	-0.207875	-0.206938	-0.20681	-0.206699
1.4	-0.20252	-0.202079	-0.201283	-0.201153	-0.201033
1.5	-0.19684	-0.196481	-0.195788	-0.195657	-0.19553
1.6	-0.19138	-0.191081	-0.190465	-0.190333	-0.190201
1.7	-0.186133	-0.185878	-0.185319	-0.18519	-0.185055
1.8	-0.181091	-0.180869	-0.180356	-0.180228	-0.180093
1.9	-0.176248	-0.176051	-0.175574	-0.17545	-0.175316
2	-0.171597	-0.171419	-0.170972	-0.170853	-0.170722
2.1	-0.167131	-0.166967	-0.166548	-0.166433	-0.166306
2.2	-0.162843	-0.162691	-0.162295	-0.162185	-0.162064
2.3	-0.158726	-0.158583	-0.15821	-0.158105	-0.15799
2.4	-0.154772	-0.154638	-0.154285	-0.154186	-0.154076

Table E.4: Potential energy values of nematic state with various values of λ and $6 \leq \alpha \leq 9$ at the first excited LL.

λ	$\alpha = 6$	$\alpha = 7$	$\alpha = 8$	$\alpha = 9$
0.4	-0.259985	-0.259987	-0.259454	-0.258167
0.5	-0.25421	-0.254136	-0.253801	-0.252922
0.6	-0.248453	-0.248327	-0.248113	-0.247499
0.7	-0.242585	-0.242428	-0.242282	-0.24184
0.8	-0.2366	-0.23643	-0.236321	-0.235989
0.9	-0.230544	-0.230373	-0.230281	-0.23002
1	-0.224474	-0.224309	-0.224224	-0.22401

Table E.5: Potential energy values of nematic state with different values of λ and $1 \leq \alpha \leq 5$ at second excited LL. Note that $\alpha = 1$ is the isotropic phase.

λ	$\alpha = 1$	$\alpha = 2$	$\alpha = 3$	$\alpha = 4$	$\alpha = 5$
0.3	-0.295442	-0.386453	-0.532874	-0.579031	-0.729281
0.4	-0.270953	-0.315039	-0.418618	-0.432485	-0.508915
0.5	-0.24991	-0.27664	-0.33743	-0.34368	-0.371183
0.6	-0.233572	-0.251629	-0.285935	-0.288078	-0.295073
0.7	-0.220971	-0.233268	-0.252836	-0.252884	-0.252245
0.8	-0.210922	-0.21928	-0.230533	-0.229764	-0.226704
0.9	-0.202636	-0.208335	-0.214819	-0.213849	-0.210427
1	-0.195601	-0.19952	-0.20325	-0.20233	-0.199298
1.1	-0.18947	-0.192197	-0.194334	-0.193545	-0.191103
1.2	-0.183996	-0.185916	-0.187131	-0.186486	-0.184613
1.3	-0.179004	-0.180371	-0.181052	-0.180537	-0.179136
1.4	-0.174371	-0.175355	-0.175725	-0.175316	-0.174279
1.5	-0.170016	-0.170728	-0.170916	-0.170591	-0.169823
1.6	-0.165884	-0.166401	-0.16648	-0.166221	-0.165646
1.7	-0.161939	-0.162314	-0.162326	-0.162117	-0.16168
1.8	-0.158157	-0.158427	-0.158398	-0.158225	-0.157886
1.9	-0.154521	-0.154713	-0.154658	-0.154513	-0.154242

Table E.6: Potential energy values of nematic state with various values of λ and $6 \leq \alpha \leq 9$ at the second excited LL.

λ	$\alpha = 6$	$\alpha = 7$	$\alpha = 8$	$\alpha = 9$
0.3	-0.770764	-0.817992	-0.862217	-0.978162
0.4	-0.525923	-0.512759	-0.51935	-0.546955
0.5	-0.373164	-0.367503	-0.361425	-0.364713
0.6	-0.292919	-0.290583	-0.284733	-0.281967
0.7	-0.249282	-0.248299	-0.244201	-0.240779
0.8	-0.22402	-0.22373	-0.220972	-0.218348
0.9	-0.208337	-0.208386	-0.206553	-0.204844
1	-0.197794	-0.197978	-0.196778	-0.19575
1.1	-0.190067	-0.190281	-0.189504	-0.188908
1.2	-0.183916	-0.18411	-0.18361	-0.183262
1.3	-0.178668	-0.178825	-0.178501	-0.178288
1.4	-0.173962	-0.17408	-0.173865	-0.173721
1.5	-0.169603	-0.169686	-0.169538	-0.169428
1.6	-0.165488	-0.165542	-0.165435	-0.16534
1.7	-0.161559	-0.161592	-0.16151	-0.161423
1.8	-0.157789	-0.157806	-0.157739	-0.157656
1.9	-0.154161	-0.154165	-0.154108	-0.154028

Table E.7: Total energy values of nematic state with various values of λ and $1 \leq \alpha \leq 5$ at the second excited LL. Note that $\alpha = 1$ is the isotropic phase.

λ	$\alpha = 1$	$\alpha = 2$	$\alpha = 3$	$\alpha = 4$	$\alpha = 5$
0.3	-0.191643	-0.256704	-0.359876	-0.358458	-0.459404
0.4	-0.132555	-0.142041	-0.187954	-0.138388	-0.149079
0.5	-0.076912	-0.060393	-0.0491	0.023941	0.078612
0.6	-0.025974	0.007868	0.060061	0.153067	0.244681
0.7	0.021226	0.069478	0.150826	0.261786	0.377468
0.8	0.065875	0.126716	0.230795	0.358429	0.492968
0.9	0.108761	0.180911	0.304176	0.447868	0.599204
1	0.150395	0.232975	0.37341	0.532912	0.700292
1.1	0.191126	0.283548	0.439993	0.615221	0.798446
1.2	0.231199	0.333078	0.504861	0.695804	0.894894
1.3	0.270791	0.381872	0.568606	0.775277	0.990331
1.4	0.310024	0.430138	0.6316	0.854022	1.08515
1.5	0.348978	0.478015	0.694075	0.932271	1.17956
1.6	0.38771	0.525591	0.756177	1.01017	1.2737
1.7	0.426254	0.572928	0.817996	1.08779	1.36762
1.8	0.464636	0.620065	0.87959	1.16521	1.46138
1.9	0.502872	0.667028	0.940997	1.24245	1.55498

Table E.8: Total energy values of nematic state with various values of λ and $6 \leq \alpha \leq 9$ at the second excited LL.

λ	$\alpha = 6$	$\alpha = 7$	$\alpha = 8$	$\alpha = 9$
0.3	-0.450718	-0.447282	-0.440534	-0.505301
0.4	-0.099194	-0.018479	0.042894	0.083527
0.5	0.160246	0.250348	0.34138	0.423389
0.6	0.347174	0.450838	0.558633	0.663755
0.7	0.497493	0.616692	0.739725	0.862564
0.8	0.629437	0.76483	0.903516	1.04262
0.9	0.751802	0.903744	1.0585	1.21374
1	0.869028	1.03772	1.20883	1.38045
1.1	0.983436	1.16899	1.35667	1.54492
1.2	1.09627	1.29873	1.50312	1.70818
1.3	1.2082	1.42759	1.64879	1.87078
1.4	1.31959	1.5559	1.79399	2.03297
1.5	1.43063	1.68386	1.93888	2.19488
1.6	1.54143	1.81158	2.08354	2.35659
1.7	1.65204	1.9391	2.22803	2.51813
1.8	1.76249	2.06646	2.37236	2.67951
1.9	1.8728	2.19367	2.51655	2.84076

REFERENCES

[1] R. Morf and B. Halperin, Phys. Rev. B **33**, 2221 (1986).

[2] M. P. Lilly, K. B. Cooper, J. P. Eisenstein, L. N. Pfeiffer, and K. W. West, Phys. Rev. Lett. **82**, 394 (1999).

[3] R. R. Du, H. Störmer, D. Tsui, L. N. Pfeiffer, and K. West, Solid State Commun. **109**, 389 (1999).

[4] R. Côte, C. B. Doiron, J. Bourassa, and H. A. Fertig, Phys. Rev. B **68**, 155327 (2003).

[5] R. Côte and A. H. MacDonald, Phys. Rev. B **44**, 8759 (1991).

[6] E. Fradkin and S. A. Kivelson, Phys. Rev. B **59** (1999).

[7] E. Fradkin, S. A. Kivelson, E. Manousakis, and K. Nho, Phys. Rev. Lett. **84**, 1982 (2000).

[8] C. Wexler and A. Dorsey, Phys. Rev. B **64**, 115312 (2001).

[9] K. B. Cooper, M. P. Lilly, J. P. Eisenstein, L. N. Pfeiffer, and K. W. West, Phys. Rev. B **65**, 241313(R) (2002).

[10] J. K. Jain, Phys. Rev. Lett. **63**, 199 (1989).

[11] B. Halperin, P. Lee, and N. Read, Phys.Rev. B **47**, 7312 (1993).

[12] E. Rezayi and N. Read, Phys. Rev. Lett. **72**, 900 (1994).

[13] R. B. Laughlin, Phys. Rev. Lett. **50**, 1395 (1983).

[14] O. Ciftja and S. Fantoni, Phys. Rev. B **58**, 7898 (1998).

[15] V. Oganesyan, S. A. Kivelson, and E. Fradkin, Phys. Rev. B **64**, 195109 (2001).

[16] F. Zhang and S. D. Sarma, Phys. Rev. B **33**, 2903 (1986).

[17] N. Trivedi and J. Jain, Mod. Phys. Lett. B **5**, 503 (1993).

[18] D. Tsui, H. Störmer, and A. Gossard, Phys. Rev. Lett. **48**, 1559 (1982).

[19] H. Störmer et al., Phys. Rev. Lett **50**, 1953 (1983).

[20] D. Tsui and H. Störmer, IEEE J. Quantum Electron **QE-22**, 1711 (1986).

[21] R. Clark, Phys. Scr. **T39**, 45 (1991).

[22] V. Pudalov and S. Semenchinsky, JETP Lett. **39**, 170 (1984).

[23] G. Gavrilov, Z. Kvon, I. V. Kukushkin, and V. B. Timofeev, JETP Lett. **39**, 507 (1984).

[24] D. Tsui, H. Störmer, and A. Gossard, Phy. Rev. Lett. **48**, 1559 (1982).

[25] H. Störmer, Physica **B177**, 401 (1992).

[26] H. S. rmer, Phys. Scr. , 168 (1992).

[27] R. Laughlin, Phys. Rev. B **23**, 5632 (1981).

[28] R. B. Laughlin, Surf. Sci. **142**, 163 (1984).

[29] B. I. Halperin, Helv. Phys. Acta **56**, 75 (1983).

[30] R. E. Prange and S. M. Girvin, *The Quantum Hall Effect*, Springer-Verlag, 1987.

[31] J. M. Caillol, D. Levesque, J. J. Weis, and J. P. Hansen, J. Stat. Phys. **28**, 325 (1982).

[32] J. Hansen and D. Levesque, J. Phys. C **14**, L603 (1981).

[33] J. Zabolitzky, Avd. Nucl. Phys. **12**, 1 (1981).

[34] T. Chakraborty and P. Pietilainen, *The Quantum Hall Effects Fractional and Integral*, Second edition, 1995.

[35] R. Jackiw and S.-Y. Pi, Phys. Rev. D **42**, 3500 (1990).

[36] S. D. Sarma and A. Pinczuk, *Perspectives in Quantum Hall Effects*, Wiley, 1997.

[37] G. Moore and N. Read, Nucl. Phys. B **360**, 362 (1991).

[38] J. K. Jain, Phys. Rev. B **41**, 7653 (1991).

[39] A. Lopez and E. Fradkin, Phys. Rev. B **44**, 5246 (1991).

[40] D. P. Arovas, R. Schrieffer, F. Wilczek, and A. Zee, Nucl. Phys. B **251**, 117 (1985).

[41] A. L. Fetter, C. B. Hanna, and R. B. Laughlin, Phys. Rev. B **39**, 9679 (1989).

[42] R. L. Willet et al., Phys. Rev. Lett **65**, 112 (1990).

[43] R. L. Willet, R. R. Ruel, and L. N. Pfeiffer, Phys. Rev. Lett **71**, 3846 (1993).

[44] P. de Gennes and J. Prost, *The Physics of Liquid Crystals*, Clarendon Press, 1993.

[45] M. Folger, A. Koulakov, and B. Shklovskii, Phys. Rev. Lett. **76**, 499 (1996).

[46] M. Folger, A. Koulakov, and B. Shklovskii, Phys. Rev. B **54**, 1853 (1996).

[47] R. Moessner and J. Chalker, Phys. Rev. B **54**, 5006 (1996).

[48] S. A. Kivelson, E. Fradkin, and V. J. Emery, Nature (London) **393**, 550 (1998).

[49] A. M. Ettohami, C. B. Doiron, F. D. Klironomos, R. Côte, and A. T. Dorsey, Phys. Rev. Lett. **96**, 196802 (2006).

[50] S. Fantoni and S. Rosati, Nuovo Cimento Lett. **10**, 545 (1974).

[51] E. Krotscheck and M. L. Ristig, Nucl.Phys. A **242**, 389 (1975).

[52] E. Manousakis, S. Fantoni, V. R. Pandharipande, and Q. N. Usmani, Phys. Rev. B **28**, 3770 (1983).

[53] A. H. MacDonald and S. M. Girvin, Phys. Rev. B **33**, 4009 (1986).

[54] O.Ciftja and C. Wexler, Phys. Rev. B **65**, 205307 (2002).

[55] N. Gronbech-Jensen, Comp. Phys. Comm. **119**, 115 (1999).

[56] J. Lekner, Physica A **157**, 826 (1989).

[57] N. Metropolis, A. W. Rosenbluth, M. N. Rosenbluth, A. M. Teller, and E. Teller, J. Chem. Phys. **21**, 1087 (1953).

[58] D. Ceperley, G. V. Chester, and M. H. Kalos, Phys. Rev. B **16**, 3081 (1977).

[59] D. P. Landau and K. Binder, *A Guide to Monte Carlo Simulations in Statistical Physics*, Cambridge University Press, 2000.

[60] E. H. Rezayi, F. D. M. Haldane, and K. Yang, Phys. Rev. Lett **83**, 1219 (1999).

BIOGRAPHICAL SKETCH

Quoc M Doan

Research Interests

- Condensed Matter Theory
- High Accuracy Numerical and Parallel Computational Methods
- Simulation of Physical Systems

Education

- 2000 - present: Florida State University (FSU), Tallahassee, Florida
  Ph.D. in Physics, 12/2007
  M.S. in Physics 12/2002
  Thesis title: Variational study of the nematic state of 2 DEG in a magnetic field
  Major thesis advisor: Efstratios Manousakis

- 1994 -1997: Hanoi University of Technology, Hanoi, Vietnam
  B.S. in Computer Science

- 1991 - 1994: Vietnam National University, Hanoi, Vietnam
  B.S. in Physics

Research Experience

Research Assistant, 05/2001 present
Center for Materials Research and Technology, Tallahassee, FL

- Design models for exotic quantum systems; study the problems numerically and quantitatively from different angles

- Develop numerical algorithms/methods such as Monte Carlo, Hypernetted chain, Hartree-Fock..

- Use computational techniques such as Fourier transform, high oscillatory integrals, complex matrix computation, multi-dimensional fixed point iterations..

- Implement programs using C++ and MPI for parallel-processing on Linux cluster system

- Work and familiar with different computing libraries such as Numerical Recipes and Gnu Scientific Library

Teaching Experience

Teaching Assistant, 09/2000 04/2001 and 09/2005 present
Florida State University, Tallahassee, FL

- Teach general physics labs for more than 350 students

- Present lectures, instruct students on how to do the labs properly and evaluate their work

Publications

- "Quantum nematic as ground state of a two-dimensional electron gas in a magnetic field", Quoc M Doan and Efstratios Manousakis, Physical Review B 75, 195433 (2007).

- This article has been selected for the June 4, 2007 issue of Virtual Journal of Nanoscale Science and Technology covering a focused area of frontier research

Conference Presentations

- The American Physical Society, Colorado, 03/2007 Talk "Variational studies of nematic phase of half-filled Landau level 2 dimensional electron gas (2DEG) system"

- The American Physical Society, Baltimore, 03/2006 Talk "Variational studies of quantum liquid crystal phases of 2 DEG"

Awards and Honors

- Won 2nd place at the Vietnam national universitys undergraduate research contest
- Awarded scholarships of Vietnam national university from 1991-1995
- Awarded Vietnam national scholarships for gifted high-school students from 1988-1991